PCCP

PAPER

View Article Online
View Journal | View Issue

# Intermolecular vibrational energy transfers in liquids and solids†

Cite this: *Phys. Chem. Chem. Phys.*, 2014, **16**, 13995

Hailong Chen, Xiewen Wen, Xunmin Guo and Junrong Zheng*

Received 26th March 2014,
Accepted 17th May 2014

DOI: 10.1039/c4cp01300j

www.rsc.org/pccp

Resonant and nonresonant intermolecular vibrational energy transfers in KSCN/KSC$^{13}$N/KS$^{13}$C$^{15}$N aqueous and DMF solutions and crystals are studied. Both energy-gap and temperature dependent measurements reveal some surprising results, *e.g.* inverted energy-gap dependent energy transfer rates and opposite temperature dependences of resonant and nonresonant energy transfer rates. Two competing mechanisms are proposed to be responsible for the experimental observations. The first one is the dephasing mechanism in which the measured energy transfer rate originates from the dephasing of the energy donor–acceptor coherence, and the second one is the phonon-compensation mechanism derived from the second order perturbation. It is found that both the nonresonant energy transfers in the liquids and resonant energy transfers in both liquids and solids can be well described by the first mechanism. The second mechanism explains the nonresonant energy transfers in one series of the solid samples very well.

Published on 20 May 2014. Downloaded by Peking University on 9/2/2022 10:14:10 AM.

## 1. Introduction

Vibration, as one of the three basic molecular motions, is an indispensable part of chemical transformations. Vibrational energy transfers are therefore involved in all chemical bond transformation activities in condensed phases, and play critical roles in many important phenomena in various fields, *e.g.* heat transport, chemical reaction energy dissipations, electronic excitation energy conversions and dissipations (*e.g.* in solar cells, and photosynthetic systems), and trans-membrane cell signaling. The significance of vibrational energy transfers has long been well recognized, and research on them in condensed phases started several decades ago.[1–11] However, the quantitative description of intermolecular vibrational energy transfers remains a considerable challenge, as intermolecular energy transfers are typically accompanied by intramolecular energy relaxations and many mechanisms can play roles simultaneously.[12–15]

Recently we conducted a series of intermolecular vibrational energy transfers experiments in liquids,[16–22] and found that the intermolecular energy transfers observed can be described by an equation[18] derived from the well-known correlation formalism vibrational relaxation theory.[4,14,23] However, the results are difficult to rationalize using the phonon-compensation mechanism.[15]

In this work, we performed comprehensive experiments to investigate resonant and nonresonant intermolecular vibrational energy transfers among the nitrile stretches (CN, $^{13}$CN, and $^{13}$C$^{15}$N) in the KSCN/KS$^{13}$CN/KS$^{13}$C$^{15}$N aqueous and DMF solutions and crystalline samples. From the experiments, we observed opposite temperature dependences of the nonresonant and resonant energy transfers, and inverted energy-gap dependences of nonresonant energy transfer rates. The surprising results cannot be fully explained by either the equation used in our previous work[18] or the phonon compensation mechanism derived from the 1st order perturbation.[15] Summarizing all our experimental results reported in the current and previous work,[18,19,24] we propose that the experimentally observed intermolecular vibrational energy transfers result from two competing mechanisms. The first one is the dephasing mechanism in which the observed energy transfer rate is determined by the dephasing of the energy donor–acceptor coherence. This mechanism gives rise to both resonant and nonresonant energy transfers. The other is the phonon-compensation mechanism derived from the second order perturbation (the second order coupling matrix) approach, which is only responsible for nonresonant energy transfers.

## 2. Experiments

One ps amplifier and one fs amplifier are synchronized with the same seed pulse. The ps amplifier pumps an OPA to generate ~0.8 ps (varying from 0.7 to 0.9 ps as a function of frequency) mid-IR pulses with a bandwidth of 10–35 cm$^{-1}$ in a frequency range tunable from 400 cm$^{-1}$ to 4000 cm$^{-1}$ with energy 1–40 μJ per pulse (1–10 μJ per pulse for 400 cm$^{-1}$ to 900 cm$^{-1}$ and >10 μJ per pulse for higher frequencies) at the rate of 1 KHz.

*Department of Chemistry, Rice University, Houston, TX, USA.*
*E-mail: junrong@rice.edu*

† Electronic supplementary information (ESI) available: The calculation parameters of the figures containing kinetic model calculations. See DOI: 10.1039/c4cp01300j

Published on 20 May 2014. Downloaded by Peking University on 9/2/2022 10:14:10 AM.

The ~1.5 W output from the fs amplifier is used to generate a high-intensity mid-IR and terahertz super-continuum pulse with a duration <100 fs in the frequency range from <10 $cm^{-1}$ to >3500 $cm^{-1}$ at 1 KHz. In nonlinear IR experiments, the ps IR pulse is the excitation pulse (the excitation power is adjusted based on the need and the interaction spot varies from 100 to 500 microns). The super-continuum pulse is the detection beam, which is frequency resolved by a spectrograph (resolution is 1–3 $cm^{-1}$ dependent on the frequency), yielding the detection axis of a 2D IR spectrum. Two polarizers are introduced into the path of the detection beam to selectively measure the parallel or perpendicular polarized signal relative to the excitation beam. The dependence of the rotation-free signal $P_{life} = P_{\parallel} + 2 \times P_{\perp}$ upon the pump–probe delay, where $P_{\parallel}$, and $P_{\perp}$ are parallel and perpendicular data respectively, determines the vibrational lifetime. The waiting time dependent anisotropy values are obtained from $r(t) = (P_{\parallel} - P_{\perp})/(P_{\parallel} + 2 \times P_{\perp})$. That the sample is isotropic within the laser focus spot is verified by measuring the initial anisotropy values of the sample as it is rotated relative to the polarization of the excitation beam. The THz spectra were taken from a home-built ABCD THz detection system,[25] and the Raman spectra were taken from a commercial Raman spectrometer. In the analyses of reorientation dynamics and vibrational energy transfer kinetics, the heat effects from the thiocyanate vibrational relaxations which are very small were removed, following the procedure described in our previous publication:[16] the heat signal is assumed to grow with time constants slightly slower than the lifetimes of vibrational excitations of which the relaxation generates heat. The maximum amplitude of the heat signal is the transient signal at very long waiting times when most vibrational excitations have relaxed. The time dependent heat signal calculated is then subtracted from the transient signal.

Unless specified, chemicals were purchased from Sigma-Aldrich and used without further purification. $KS^{13}C^{15}N$ and $KS^{13}CN$ were purchased from Cambridge Isotope Laboratory. The solid samples were thin films of polycrystalline $KSCN/KS^{13}CN$ and $KSCN/KS^{13}C^{15}N$ mixed crystals blended with ~50 wt% PMMA (poly(methyl methacrylate)). The function of PMMA was to suppress scattered light. In the low temperature measurements, the samples were placed in a Janis cryostat under vacuum. In the high temperature measurements, the samples were placed in a Harrick Scientific temperature control cell.

# 3. Theoretical background

The theory of energy transfers between molecules and energy relaxations in condensed phases has been addressed by a number of authors.[4,15,23,24,26–38] There are two possible limiting cases of vibrational energy transfers: $V \ll \tau^{-1}$ and $V \geq \tau^{-1}$ where $V$ is the donor–acceptor coupling strength and $\tau^{-1}$ is the homogeneous dephasing linewidth of the donor or the acceptor. Most of the present work will be concerned with the first case of resonant and near resonant energy transfers. Based on the listed pioneering work, the derivations with some phenomenological descriptions leading to energy transfer rate equations that serve as a foundation to explain our experimental results are provided in the following.

## 3.1 Dephasing mechanism

The vibrational energy transfer equation of the dephasing mechanism[36–39] can be derived from the coupled donor–acceptor pair, following our previous work[40] with some modifications. The derivation leads to an equation in which all parameters can be experimentally quantitatively determined. The system state can be expressed as

$$|\psi\rangle = c_1(t)e^{-i\omega_D t}|D = 1,A = 0\rangle + c_2(t)e^{-i\omega_A t}|D = 0,A = 1\rangle, \quad (1)$$

where $\omega_D$ and $\omega_A$ are the 0–1 transition frequencies of the donor (D) and the acceptor (A), respectively. $|D = 1,A = 0\rangle$ is the donor state where the donor is at the 1st excited state and the acceptor is at the ground state. $|D = 0,A = 1\rangle$ is the acceptor state where the donor is at the ground state and the acceptor is at the 1st excited state. $c_1(t)$ and $c_2(t)$ are the coefficients of these two states with $|c_1(t)|^2 + |c_2(t)|^2 \equiv 1$. The coupling between the two states is $V = \frac{\langle D = 1, A = 0|H|D = 0, A = 1\rangle}{\hbar} = \frac{\langle D = 0, A = 1|H|D = 1, A = 0\rangle}{\hbar}$ where $H$ is the system Hamiltonian. Substituting eqn (1) into the time dependent Schrödinger equation with the initial condition $c_1(0) = 1$; $c_2(0) = 0$, one can obtain

$$c_1(t) = e^{\frac{1}{2}i\Delta\omega t}\left[\cos\left[\frac{t}{2}\sqrt{(\Delta\omega)^2 + 4V^2}\right] - i\frac{\Delta\omega \sin\left[\frac{t}{2}\sqrt{(\Delta\omega)^2 + 4V^2}\right]}{\sqrt{(\Delta\omega)^2 + 4V^2}}\right] \quad (2)$$

$$c_2(t) = \frac{2Ve^{-\frac{1}{2}i\Delta\omega t}\sin\left(\frac{t}{2}\sqrt{(\Delta\omega)^2 + 4V^2}\right)}{\sqrt{(\Delta\omega)^2 + 4V^2}}, \quad (3)$$

where $\Delta\omega = \omega_A - \omega_D$. Here we propose that the coherence between the donor and acceptor states is terminated by an abrupt dephasing event, which is random and therefore follows the 1st order kinetics. After the dephasing event, the system stays in the acceptor state with a probability $|c_2(t_c)|^2$. The ensemble average probability on the acceptor state for a dephasing period $\tau$ is $P = \int_0^\infty |c_2(t_c)|^2 p(t_c) dt_c$, where $p(t_c) = \tau^{-1}e^{-t_c/\tau}$ is the probability of dephasing at time $t_c$ with $\int_0^\infty p(t_c)dt_c = 1$.[39] The acceptor state growth rate constant is therefore

$$k_p = \frac{P}{\tau} = 2V^2\frac{\frac{1}{\tau}}{(\Delta\omega)^2 + 4V^2 + \tau^{-2}}. \quad (4)$$

The growth rate constant $k_p = k_{DA} + k_{AD}$, where $k_{DA}$ is the energy transfer rate constant from the donor state to the acceptor state and $k_{AD}$ is the reverse constant, can be derived from the kinetic scheme $D \underset{k_{AD}}{\overset{k_{DA}}{\rightleftharpoons}} A$, where $k_{DA} = e^{-\frac{\Delta\omega}{RT}}k_{AD}$ is

 This journal is © the Owner Societies 2014

Published on 20 May 2014. Downloaded by Peking University on 9/2/2022 10:14:10 AM.

determined using the detailed balance principle and the kinetic solution is $D(t) = \frac{1}{2}e^{-(k_{DA}+k_{AD})t} + \frac{1}{2}$ and $A(t) = -\frac{1}{2}e^{-(k_{DA}+k_{AD})t} + \frac{1}{2}$ with the initial conditions D(0) = 1, and A(0) = 0. Therefore, the energy transfer rate constant from the donor state to the acceptor state is

$$k_{DA} = \frac{2}{1+e^{\frac{\Delta\omega}{RT}}} V^2 \frac{\frac{1}{\tau}}{(\Delta\omega)^2 + 4V^2 + \tau^{-2}}. \quad (5)$$

Eqn (5) is the energy transfer rate equation of the dephasing mechanism. It requires $V < \tau^{-1}$. For $V > \tau^{-1}$, the coherent energy transfer mechanism will dominate, *i.e.* a donor–acceptor exciton will persist.[24] In all the experiments reported here, $V < \tau^{-1}$. All the parameters of eqn (5) are experimentally accessible and therefore it can be quantitatively experimentally tested. An equation similar to eqn (5) can also be derived from the correlation formalism with the assumption that the vibrational coupling correlation function is a single exponential.[4,18]

If the 0–1 dephasing of the donor is uncorrelated with the 0–1 dephasing of the acceptor, another equation similar to eqn (5) can be derived in the frequency domain. Under the weak coupling limit, the probability at the acceptor state can be obtained by simplifying eqn (3) or directly from the 1st order perturbation:

$$|c_2(t)|^2 = \frac{4V^2 \sin^2\left(\frac{\Delta\omega}{2}t\right)}{(\Delta\omega)^2}. \quad (6)$$

Both the donor and acceptor 0–1 transitions are assumed to be homogeneously broadened so that both 0–1 transition lineshapes are Lorentzian with line widths $\tau_D$ and $\tau_A$ respectively. The probability of the donor at the frequency $\omega_1$ is $\frac{1}{\pi}\frac{\tau_D^{-1}}{(\omega_1-\omega_D)^2+\tau_D^{-2}}$, and that of the acceptor at the frequency $\omega_2$ is $\frac{1}{\pi}\frac{\tau_A^{-1}}{(\omega_2-\omega_A)^2+\tau_A^{-2}}$. The experimentally observed energy transfer is the sum of the transfers between all these possible donor and acceptor frequencies. Therefore, the donor–acceptor energy transfer rate constant is

$$k_{DA} = \frac{1}{1+e^{\frac{\Delta\omega}{RT}}} \times \frac{1}{t} \times \int_{-\infty}^{\infty}\int_{-\infty}^{\infty} \frac{1}{\pi} \times \frac{\tau_D^{-1}}{(\omega_x-\omega_D)^2+\tau_D^{-2}} \times \frac{1}{\pi} \times \frac{\tau_A^{-1}}{(\omega_\Delta+\omega_x-\omega_A)^2+\tau_A^{-2}} \times |c_2(t,\omega_\Delta)|^2 d\omega_x d\omega_\Delta. \quad (7)$$

Substituting eqn (6) into eqn (7) and simplifying it, we obtain

$$k_{DA} = \frac{1}{1+e^{\frac{\Delta\omega}{RT}}} \times \frac{1}{t} \times \int_{-\infty}^{\infty} \frac{1}{\pi} \times \frac{\tau_A^{-1}+\tau_D^{-1}}{[\omega_\Delta-(\omega_A-\omega_D)]^2+(\tau_A^{-1}+\tau_D^{-1})^2} \times \frac{t}{2} \times \frac{4V^2 \sin^2\left(\frac{\omega_\Delta}{2}t\right)}{\left(\frac{\omega_\Delta}{2}t\right)^2} d\left(\frac{\omega_\Delta}{2}t\right). \quad (8)$$

Eqn (8) can be transformed into

$$k_{DA} \cong \frac{2V^2}{1+e^{\frac{\Delta\omega}{RT}}} \times \frac{1}{\pi} \times \frac{\tau_A^{-1}+\tau_D^{-1}}{(\omega_A-\omega_D)^2+(\tau_A^{-1}+\tau_D^{-1})^2} \int_{-\infty}^{\infty} \frac{\sin^2\left(\frac{\omega_\Delta}{2}t\right)}{\left(\frac{\omega_\Delta}{2}t\right)^2} d\left(\frac{\omega_\Delta}{2}t\right). \quad (9)$$

The integration in eqn (9) is equal to π, so that eqn (9) becomes

$$k_{DA} = \frac{2V^2}{1+e^{\frac{\Delta\omega}{RT}}} \frac{\tau_A^{-1}+\tau_D^{-1}}{(\omega_A-\omega_D)^2+(\tau_A^{-1}+\tau_D^{-1})^2}. \quad (10)$$

Eqn (10) is the weak coupling limit of eqn (5) for the uncorrelated D/A dephasing case. It is similar to the electronic energy transfer rate equation of the hopping mechanism.[24] Comparing eqn (5) and (10), we can see that if the 0–1 transition dephasings of the donor and acceptor are uncorrelated, the energy transfer dephasing time $\tau$ in eqn (5) can be obtained from $\tau^{-1} = \tau_A^{-1} + \tau_D^{-1}$. For most cases, the intermolecular vibrational energy transfers that can be experimentally observed are expected to occur within a distance of less than 1 nm because of the relatively small vibrational transition dipole moments (0.2–0.5 D) and short vibrational lifetimes (a few to hundreds of ps). Within such short distances, the molecular factors, *e.g.* the electric field fluctuations, that cause the donor to dephase, must also affect the dephasing of the acceptor in a certain way, *vice versa*. In other words, the dephasings of the donor and acceptor are correlated. For the correlated cases, the energy transfer dephasing time $\tau$ must be longer than that of the uncorrelated case. How long $\tau$ can be is dependent on the detailed correlation, which cannot be directly obtained from a single experiment. However, according eqn (5), $\tau$ can be obtained by measuring the energy transfer rates for different energy gaps ($\Delta\omega$).

The physical picture behind eqn (5) can be deduced from the above derivations for both eqn (5) and (10): the energy transfer rate described by eqn (5) is determined by the resonant energy transfer of the portions of donor and acceptor at the same frequencies. (Different from the situation in eqn (10), the frequency overlap range is smaller in eqn (5) because of the correlated dephasings.) For a donor and an acceptor with different central frequencies ($\omega_D$ and $\omega_A$), the dephasing events inevitably cause the donor and the acceptor to have some of the same frequencies with certain probabilities. At these same frequencies, the donor and acceptor transfer energy in a resonant manner, and then the acceptor which carries the transferred energy may change its frequencies because of dephasing, spectral diffusion or chemical exchange. Such a resonant energy transfer process contributes to the overall experimentally observed nonresonant energy transfers. A smaller central frequency difference results in a larger frequency overlap and a faster energy transfer.

Similar to a previous theory,[36–38] eqn (5) also predicts a non-monotonic dephasing time dependence of energy transfer rate. When the dephasing is fast ($\tau^{-1}$ is larger than the energy gap

Published on 20 May 2014. Downloaded by Peking University on 9/2/2022 10:14:10 AM.

$\Delta\omega$ between the donor and acceptor), the energy transfer rate is roughly proportional to $\tau$ and therefore the energy transfer is slower with a faster dephasing. When the dephasing is slow ($\tau^{-1}$ is smaller than the energy gap $\Delta\omega$ between the donor and the acceptor), the energy transfer rate is roughly inversely proportional to $\tau$. The energy transfer is faster with faster dephasing. The physical pictures behind such a non-monotonic behavior can be understood from both derivations in the time and frequency domains described above: (A) when the gap is much larger than the dephasing width ($\tau^{-1}$), the energy transfer rate is limited by the probability of the donor and acceptor to be in resonance. A faster dephasing causes a larger probability of the donor and acceptor to be in resonance and therefore a faster transfer rate. (B) When the dephasing width is much larger than the gap, which implies that the donor and acceptor have significant energy overlapping and the chance for them to be in resonance is large, the energy transfer rate is limited by the donor–acceptor coherence time. A longer coherence leads to a larger probability of the excitation on the acceptor state and thus a faster energy transfer. A faster dephasing causes shorter donor–acceptor coherence and thus a slower energy transfer. One extreme case of situation (B) is the resonant energy transfer where the donor and acceptor have the same energy.

If the central frequency difference is large and the dephasing time is long, the probability of the donor and acceptor to have the same frequency is very small and the nonresonant energy transfer predicted by eqn (5) is very slow. In this situation, another energy transfer mechanism, the phonon compensation nonresonant energy transfer mechanism, can become important. Similar to the nonlinear optical effect that one photon can split into several photons or several photons can combine into one photon, energy can directly transfer in a nonresonant manner from the donor to the acceptor of a different frequency by emitting or absorbing photons into or from the environment to conserve energy. We call the nonresonant energy transfer process the phonon compensation mechanism. In this work, we will only discuss the process of emitting or absorbing one photon (phonon), or the so called "cubic" process.[15] Processes involving more phonons are typically slower and we expect that it is difficult to experimentally observe these slow processes as many competing energy transfer pathways (*e.g.* intramolecular relaxations) are much faster.

Before we go into the phonon compensation mechanism, one issue needs to be discussed. In addition to the dephasing process, inhomogeneous broadening can also cause some frequency overlapping. In a system in the condensed phase, the vibrational line width is typically the result of both processes. For a very inhomogeneous system, the decomposition of a peak into several homogeneous sub-components is needed before applying eqn (5). In reality, as determined by 2D IR, most room temperature liquid samples that have been measured contain only 10% to 30% inhomogeneous broadening contribution.[41–46] Such an amount of inhomogeneous broadening can introduce a similar amount of uncertainty in the determined energy transfer rate by directly using eqn (5). However, because the energy transfer dephasing time $\tau$ in eqn (5) is an effective (average) parameter determined by the energy-gap dependent experiments rather than from the linear absorption lineshapes, the uncertainty is expected to be smaller than the contribution of inhomogeneous broadening to the total line width. In addition, the energy transfer dephasing time $\tau$ determined by this method already contains the contribution of spectral diffusion.

### 3.2 Phonon compensation mechanism

Nonresonant vibrational relaxations or transfers compensated with phonons from the bath were theoretically described previously.[15,47,48] For the one-phonon process (the cubic process) of nonresonant intermolecular vibrational energy transfers, in contrast to the previous work[15] where nonresonant energy transfers were treated as a process directly from the donor state to the acceptor state, the derivation in the following requires virtual intermediate states between the donor and acceptor states. The difference in mechanism results in a different energy transfer rate equation.

The derivation follows the theory of nonresonant electronic energy transfers of impurities in solids.[32] According to the golden rule, the transition probability per unit time for excitation transfer to take place is

$$k_{\mathrm{fi}} = \frac{2\pi}{\hbar}|W_{\mathrm{fi}}|^2\rho(E_{\mathrm{fi}}), \tag{11}$$

where $W_{\mathrm{fi}}$ is the coupling matrix element, and $\rho(E)$ is the density of states. The coupling matrix can be expanded to the second-order (higher orders which may require more than one phonon are omitted)

$$W_{\mathrm{fi}} = \langle \mathrm{f}|H'|\mathrm{i}\rangle + \sum_{\mathrm{m}} \frac{\langle \mathrm{f}|H'|\mathrm{m}\rangle\langle \mathrm{m}|H'|\mathrm{i}\rangle}{E_{\mathrm{i}} - E_{\mathrm{m}}}, \tag{12}$$

where $|\mathrm{i}\rangle$ and $|\mathrm{f}\rangle$ are the initial and final states, respectively, and $|\mathrm{m}\rangle$ denotes all possible intermediate states. $E_{\mathrm{i}}$ and $E_{\mathrm{m}}$ are the total energy of the states $|\mathrm{i}\rangle$ and $|\mathrm{m}\rangle$ respectively. The coupling Hamiltonian $H'$ consists of direct interactions between the donor and the acceptor $H_{\mathrm{DA}}$ (*e.g.* dipole–dipole interactions if the distance is sufficiently large) and the coupling between the system (energy donor and acceptor) and the phonons $H_{\mathrm{ph}}(\mathrm{D})$, $H_{\mathrm{ph}}(\mathrm{A})$:

$$H' = H_{\mathrm{DA}} + H_{\mathrm{ph}}(\mathrm{D}) + H_{\mathrm{ph}}(\mathrm{A}). \tag{13}$$

We have the initial state where the donor D is at its first excited state D*, the acceptor A is at the ground state A, and the phonon state is $n_{\mathbf{q}}$

$$|\mathrm{i}\rangle = |\mathrm{D}^*,\mathrm{A},n_{\mathbf{q}}\rangle, \tag{14}$$

and the final state where the donor D is at the ground state D, the acceptor A is at its first excited state A*, and the phonon state is $n_{\mathbf{q}} \pm 1$

$$|\mathrm{f}\rangle = |\mathrm{D},\mathrm{A}^*,n_{\mathbf{q}} \pm 1\rangle, \tag{15}$$

with an equal energy $E_{\mathrm{i}}$. The energy gap between the donor and acceptor $\Delta E = E_{\mathrm{D}} - E_{\mathrm{A}}$ is made up of one phonon, and the upper

 This journal is © the Owner Societies 2014

Published on 20 May 2014. Downloaded by Peking University on 9/2/2022 10:14:10 AM.

and lower signs designate phonon emission $\Delta E > 0$ and absorption $\Delta E < 0$, respectively. The two possible intermediate states are

$$|\mathrm{m}_1\rangle = |\mathrm{D}^*,\mathrm{A},n_{\mathbf{q}} \pm 1\rangle, \tag{16}$$

$$|\mathrm{m}_2\rangle = |\mathrm{D},\mathrm{A}^*,n_{\mathbf{q}}\rangle. \tag{17}$$

with energies $E_\mathrm{i} + \Delta E$ and $E_\mathrm{i} - \Delta E$ respectively. $\mathbf{q}$ denotes the wave vector of the phonon, with energy $\hbar\cdot\omega(\mathbf{q}) = |\Delta E|$.

The first order coupling matrix element is negligibly small, as

$$\begin{aligned}\langle \mathrm{f}|H'|\mathrm{i}\rangle &= \left\langle \mathrm{D},\mathrm{A}^*,n_{\mathbf{q}} \pm 1\middle|H_{\mathrm{DA}} + H_{\mathrm{ph}}(\mathrm{D}) + H_{\mathrm{ph}}(\mathrm{A})\middle|\mathrm{D}^*,\mathrm{A},n_{\mathbf{q}}\right\rangle \\ &= \left\langle \mathrm{D},\mathrm{A}^*,n_{\mathbf{q}} \pm 1\middle|H_{\mathrm{DA}}\middle|\mathrm{D}^*,\mathrm{A},n_{\mathbf{q}}\right\rangle \\ &\quad + \left\langle \mathrm{D},\mathrm{A}^*,n_{\mathbf{q}} \pm 1\middle|H_{\mathrm{ph}}(\mathrm{D})\middle|\mathrm{D}^*,\mathrm{A},n_{\mathbf{q}}\right\rangle \\ &\quad + \left\langle \mathrm{D},\mathrm{A}^*,n_{\mathbf{q}} \pm 1\middle|H_{\mathrm{ph}}(\mathrm{A})\middle|\mathrm{D}^*,\mathrm{A},n_{\mathbf{q}}\right\rangle. \\ &= \langle \mathrm{D},\mathrm{A}^*|H_{\mathrm{DA}}|\mathrm{D}^*,\mathrm{A}\rangle\langle n_{\mathbf{q}} \pm 1 \mid n_{\mathbf{q}}\rangle \\ &\quad + \left\langle n_{\mathbf{q}} \pm 1\middle|H_{\mathrm{ph}}(\mathrm{D})\middle|n_{\mathbf{q}}\right\rangle\langle \mathrm{D},\mathrm{A}^* \mid \mathrm{D}^*,\mathrm{A}\rangle \\ &\quad + \left\langle n_{\mathbf{q}} \pm 1\middle|H_{\mathrm{ph}}(\mathrm{A})\middle|n_{\mathbf{q}}\right\rangle\langle \mathrm{D},\mathrm{A}^* \mid \mathrm{D}^*,\mathrm{A}\rangle \\ &= \langle \mathrm{D},\mathrm{A}^*|H_{\mathrm{DA}}|\mathrm{D}^*,\mathrm{A}\rangle \times 0 + \left\langle n_{\mathbf{q}} \pm 1\middle|H_{\mathrm{ph}}(\mathrm{D})\middle|n_{\mathbf{q}}\right\rangle \\ &\quad \times 0 + \left\langle n_{\mathbf{q}} \pm 1\middle|H_{\mathrm{ph}}(\mathrm{A})\middle|n_{\mathbf{q}}\right\rangle \times 0 \\ &= 0.\end{aligned} \tag{18}$$

The second order matrix element can be expanded into

$$\sum_\mathrm{m} \frac{\langle \mathrm{f}|H'|\mathrm{m}\rangle\langle \mathrm{m}|H'|\mathrm{i}\rangle}{E_\mathrm{i} - E_\mathrm{m}} = \frac{\langle \mathrm{D},\mathrm{A}^*|H_{\mathrm{DA}}|\mathrm{D}^*,\mathrm{A}\rangle\left(\left\langle \mathrm{D}^*,n_{\mathbf{q}} \pm 1\middle|H_{\mathrm{ph}}(\mathrm{D})\middle|\mathrm{D}^*,n_{\mathbf{q}}\right\rangle + \left\langle \mathrm{A},n_{\mathbf{q}} \pm 1\middle|H_{\mathrm{ph}}(\mathrm{A})\middle|\mathrm{A},n_{\mathbf{q}}\right\rangle\right)}{-\Delta E} + \frac{\left(\left\langle \mathrm{D},n_{\mathbf{q}} \pm 1\middle|H_{\mathrm{ph}}(\mathrm{D})\middle|\mathrm{D},n_{\mathbf{q}}\right\rangle + \left\langle \mathrm{A}^*,n_{\mathbf{q}} \pm 1\middle|H_{\mathrm{ph}}(\mathrm{A})\middle|\mathrm{A}^*,n_{\mathbf{q}}\right\rangle\right)\langle \mathrm{D},\mathrm{A}^*|H_{\mathrm{DA}}|\mathrm{D}^*,\mathrm{A}\rangle}{\Delta E} \tag{19}$$

The matrix elements in eqn (19) can be written as

$$\begin{aligned}\langle \mathrm{D},\mathrm{A}^*|H_{\mathrm{DA}}|\mathrm{D}^*,\mathrm{A}\rangle &= V \\ \left\langle \mathrm{D},n_{\mathbf{q}} \pm 1\middle|H_{\mathrm{ph}}(\mathrm{D})\middle|\mathrm{D},n_{\mathbf{q}}\right\rangle &= g_\mathrm{D}(s,q)\cdot\left\langle n_{\mathbf{q}} \pm 1\middle|\left(b^\dagger_{s,q} + b_{s,-q}\right)\middle|n_{\mathbf{q}}\right\rangle \\ &\quad \times \exp(\mp\mathrm{i}\mathbf{q}\cdot\mathbf{r}_\mathrm{D}) \\ \left\langle \mathrm{A},n_{\mathbf{q}} \pm 1\middle|H_{\mathrm{ph}}(\mathrm{A})\middle|\mathrm{A},n_{\mathbf{q}}\right\rangle &= g_\mathrm{A}(s,q)\cdot\left\langle n_{\mathbf{q}} \pm 1\middle|\left(b^\dagger_{s,q} + b_{s,-q}\right)\middle|n_{\mathbf{q}}\right\rangle \\ &\quad \times \exp(\mp\mathrm{i}\mathbf{q}\cdot\mathbf{r}_\mathrm{A}) \\ \left\langle \mathrm{D}^*,n_{\mathbf{q}} \pm 1\middle|H_{\mathrm{ph}}(\mathrm{D})\middle|\mathrm{D}^*,n_{\mathbf{q}}\right\rangle &= e_\mathrm{D}(s,q)\cdot\left\langle n_{\mathbf{q}} \pm 1\middle|\left(b^\dagger_{s,q} + b_{s,-q}\right)\middle|n_{\mathbf{q}}\right\rangle \\ &\quad \times \exp(\mp\mathrm{i}\mathbf{q}\cdot\mathbf{r}_\mathrm{D}) \\ \left\langle \mathrm{A}^*,n_{\mathbf{q}} \pm 1\middle|H_{\mathrm{ph}}(\mathrm{D})\middle|\mathrm{A}^*,n_{\mathbf{q}}\right\rangle &= e_\mathrm{A}(s,q)\cdot\left\langle n_{\mathbf{q}} \pm 1\middle|\left(b^\dagger_{s,q} + b_{s,-q}\right)\middle|n_{\mathbf{q}}\right\rangle \\ &\quad \times \exp(\mp\mathrm{i}\mathbf{q}\cdot\mathbf{r}_\mathrm{A}),\end{aligned} \tag{20}$$

where $g_\mathrm{i}(s,q)$ and $e_\mathrm{i}(s,q)$ (i = D, A) denote the coupling to the phonon of wave vector $\mathbf{q}$ (branch $s$) for the ground state and the 1st excited state, respectively. $b^\dagger_{s,q}$, and $b_{s,-q}$ are the phonon creation and annihilation operators. $\mathbf{r}_\mathrm{D}$ and $\mathbf{r}_\mathrm{A}$ are the position vectors of donor and acceptor. Inserting eqn (18)–(20) into eqn (12), one can obtain

$$\begin{aligned}W_{\mathrm{fi}}(\mathbf{q}) &= \frac{V}{-\Delta E}\cdot\left\langle n_{\mathbf{q}} \pm 1\middle|\left(b^\dagger_{s,q} + b_{s,-q}\right)\middle|n_{\mathbf{q}}\right\rangle\cdot[e_\mathrm{D}(s,q)\cdot\exp(\mp\mathrm{i}\mathbf{q}\cdot\mathbf{r}_\mathrm{D}) \\ &\quad + g_\mathrm{A}(s,q)\cdot\exp(\mp\mathrm{i}\mathbf{q}\cdot\mathbf{r}_\mathrm{A})] \\ &\quad + \frac{V}{\Delta E}\cdot\left\langle n_{\mathbf{q}} \pm 1\middle|\left(b^\dagger_{s,q} + b_{s,-q}\right)\middle|n_{\mathbf{q}}\right\rangle\cdot[g_\mathrm{D}(s,q)\cdot\exp(\mp\mathrm{i}\mathbf{q}\cdot\mathbf{r}_\mathrm{D}) \\ &\quad + e_\mathrm{A}(s,q)\cdot\exp(\mp\mathrm{i}\mathbf{q}\cdot\mathbf{r}_\mathrm{A})]\end{aligned} \tag{21}$$

We define $\mathbf{r} = \mathbf{r}_\mathrm{A} - \mathbf{r}_\mathrm{D}$ as the distance vector between the donor and acceptor. If the donor and acceptor have very similar molecular properties, $g_\mathrm{D}(s,q) \cong g_\mathrm{A}(s,q)$ and $e_\mathrm{D}(s,q) \cong e_\mathrm{A}(s,q)$. We define $V_{\mathrm{ph}}(s,q) = g_\mathrm{D}(s,q) - e_\mathrm{D}(s,q) = g_\mathrm{A}(s,q) - e_\mathrm{A}(s,q)$. Under the conditions, eqn (21) can be rewritten as

$$\begin{aligned}W_{\mathrm{fi}}(\mathbf{q}) &= \frac{V}{\Delta E}\cdot\left\langle n_{\mathbf{q}} \pm 1\middle|\left(b^\dagger_{s,q} + b_{s,-q}\right)\middle|n_{\mathbf{q}}\right\rangle\cdot V_{\mathrm{ph}}(s,q) \\ &\quad \times \exp(\mp\mathrm{i}\mathbf{q}\cdot\mathbf{r}_\mathrm{A})\cdot[\exp(\pm\mathrm{i}\mathbf{q}\cdot\mathbf{r}) - 1].\end{aligned} \tag{22}$$

The phonon transition term is

$$\left\langle n_{\mathbf{q}} \pm 1\middle|\left(b^\dagger_{s,q} + b_{s,-q}\right)\middle|n_{\mathbf{q}}\right\rangle = \begin{cases}\sqrt{n(s,q)+1} \\ \sqrt{n(s,q)}\end{cases}\text{for}\begin{cases}\text{emission} \\ \text{absorption}\end{cases}, \tag{23}$$

where $n(s,q) = n(\Delta E,T) = [\exp(|\Delta E|/k_\mathrm{B}T) - 1]^{-1}$ is the Boson thermal occupation number, and $k_\mathrm{B}$ is Boltzmann's constant. Inserting eqn (22) and (23) into eqn (11), one can obtain the energy transfer rate constant from the initial state to the final state

$$k'_{\mathrm{fi}} = \frac{2\pi}{\hbar}\cdot\frac{|V|^2}{\Delta E^2}\cdot\rho_{\mathrm{eff}}(\Delta E)\cdot(n(\Delta E,T)+1) \tag{24}$$

for the emission process ($\Delta E > 0$), and

$$k'_{\mathrm{fi}} = \frac{2\pi}{\hbar}\cdot\frac{|V|^2}{\Delta E^2}\cdot\rho_{\mathrm{eff}}(\Delta E)\cdot n(\Delta E,T) \tag{25}$$

for the absorption process ($\Delta E < 0$), where $\rho_{\mathrm{eff}}(\Delta E) = \sum_\mathrm{s}|V_{\mathrm{ph}}(s,q)|^2\cdot|\exp(\mathrm{i}\mathbf{q}\cdot\mathbf{r}) - 1|^2\cdot\rho_\mathrm{s}(\Delta E)$ is the effective phonon density of states weighted by the coupling parameter difference. Eqn (24) and (25) are the vibrational energy transfer rate equations of the one-phonon compensation mechanism. The essential difference

Published on 20 May 2014. Downloaded by Peking University on 9/2/2022 10:14:10 AM.

between these equations and the equations in the previous theory assuming the direct energy transfer from the donor to the acceptor[15] is that in eqn (24) and (25) there is a term $\Delta E^2$ in the denominator.

From the derivation, we can see that a few conditions are required for the energy transfer through this mechanism to be nontrivial. The first one is that the density of states $\rho_s(\Delta E)$ must be reasonably large. The second one is that the coherence term $|\exp(i\mathbf{q}\cdot\mathbf{r}) - 1|^2$ must be nonzero. The physical picture behind this term is that the donor and the acceptor must be so far away that the modulations of the phonon on them are different. This condition can be approximately fulfilled for nonresonant vibrational energy transfers with gaps smaller than RT ($\sim$200 cm$^{-1}$ at room temperature) because both the phonon wavelength and the donor–acceptor distance are at the scale of a few angstroms. The third one is that $|V_{ph}(s,q)|^2$ must be non-zero. In other words, it requires a difference in the couplings of a phonon to the vibrational excited state and the ground state of the same molecule.

### 3.3 Comparisons between the two mechanisms

**3.3.1 The energy gap dependence.** One major difference between the two mechanisms is that in the dephasing mechanism the energy transfer is slower with a larger energy gap, but in the phonon compensation mechanism this is not necessarily the case. As described by eqn (5), for nonresonant energy transfers with the energy gap ($\Delta\omega$) larger than the dephasing width ($\tau^{-1}$), the energy transfer rate constant becomes approximately inversely proportional to the square of energy gap because the coupling strength ($V$) and dephasing time ($\tau$) are hardly affected by the relatively small energy gap (*e.g.* $<$200 cm$^{-1}$ at RT). However, according to eqn (24) and (25), the energy transfer rate is not only determined by the energy gap, but also by the phonon density of states ($\rho_s(\Delta E)$) and the phonon/system coupling ($V_{ph}(s,q)$) all of which are sensitive to the energy gap. Dependent on the detailed values of these two parameters, the energy transfer rates with two different energy gaps can be the same or different in either way. Experimentally, the difference in the energy gap dependences of the two mechanisms can be tested.

**3.3.2 The temperature dependence.** The energy transfer rates from both mechanisms are temperature dependent. Here we assume that the direct donor–acceptor vibrational coupling (*e.g.* transition dipole–transition dipole interaction) is hardly affected by the temperature change if no phase transition or chemical transformation occurs. In the dephasing mechanism (eqn (5)), the temperature change causes the dephasing time $\tau$ to change. Typically, at a higher temperature, molecular motions are faster and the dephasing time is shorter. According to eqn (5), for the resonant energy transfer, the rate will become slower at a higher temperature, but for a nonresonant energy transfer with the energy gap ($\Delta\omega$) larger than the dephasing width ($\tau^{-1}$) the rate will increase as the temperature rises. The physical picture behind the opposite temperature dependences of the resonant and nonresonant energy transfers is that a faster dephasing leads to a shorter donor–acceptor coherence between the donor and the acceptor, but a larger probability of frequency overlap if the central frequencies of donor and acceptor are off resonance. A shorter coherence leads to a slower resonant energy transfer, but a larger frequency overlap leads to a larger probability of energy transfer from the off-resonant donor to the acceptor. In the phonon compensation mechanism, according to eqn (24) and (25), the temperature effect reflects on the temperature dependent Boson occupation number. For the down-flowing ($\omega_D > \omega_A$) energy transfer process, the temperature dependence of energy transfer rate is $k_{DA}(T) \propto \frac{1}{\exp(|\Delta E|/k_B T) - 1} + 1$ which states that a higher temperature leads to a faster nonresonant energy transfer. Summarizing the above discussions, both mechanisms suggest that the nonresonant energy transfer is faster at a higher temperature, in contrast to the resonant energy transfer. The difference between the two mechanisms is that the temperature dependence of the phonon compensation mechanism is a well-defined function if the density of states is temperature independent, but that of the dephasing mechanism is not as quantitative. The temperature dependences of energy transfer rate can be experimentally tested.

**3.3.3 The quantitative level.** Eqn (5) can be experimentally quantitatively tested. The energy transfer rate constant ($k_{DA}$) can be determined from the energy transfer experiments through the vibrational energy exchange method or the anisotropy decay method.[49] The energy gap ($\Delta\omega$) can be determined with FTIR, and the dephasing time can be indirectly determined by the energy gap dependent energy transfer experiments. The remaining parameter, the coupling strength ($V$), can be determined through the transition dipole–transition dipole interaction[50]

$$V^2 = \frac{1}{n^4}\frac{{\mu_D}^2{\mu_A}^2}{(4\pi\varepsilon_0)^2}\frac{\kappa^2}{{r_{DA}}^6}, \quad (26)$$

where $n$ is the refractive index which may need a local field correction factor for some cases.[50] $\varepsilon_0$ is the vacuum permittivity. $\mu_D$ and $\mu_A$ are the transition dipole moments of the donor and acceptor respectively. $r_{DA}$ is the distance between the donor and acceptor. $\kappa$ is the orientation factor determined by the relative orientations of the donor and the acceptor. Eqn (26) requires $r_{DA}$ to be larger than the sizes of the donor and acceptor in order to obtain a reasonably precise result,[51] which can be fulfilled in many intermolecular vibrational energy transfers between two relatively localized modes, because in these cases $r_{DA}$ is between 2 and 10 angstroms and the sizes of the vibrational modes are 1–2 angstroms which is the length of a typical chemical bond. Combining eqn (5) and (26), one can quantitatively test the validity of eqn (5) with samples of well-defined donor–acceptor distances and orientations, or derive the donor–acceptor distances from the vibrational energy transfer measurements.

In contrast to eqn (5), (24) and (25) are difficult to experimentally quantitatively evaluate, because the phonon density of states ($\rho_s(\Delta E)$) and the phonon/system coupling ($V_{ph}(s,q)$) are difficult to experimentally quantitatively determine. Estimates of the general phonon density of states (energy $<$ 200 cm$^{-1}$) can be experimentally obtained from combinations of far IR (or THz) absorption, Raman, and neutron scattering experiments, but not

 This journal is © the Owner Societies 2014

Published on 20 May 2014. Downloaded by Peking University on 9/2/2022 10:14:10 AM.

all experimentally measured phonons may be involved in the energy transfer process and not all phonons involved are experimentally accessible. Therefore, the effective phonons and their coupling strengths to the energy transfer systems can at most be estimated. To semi-quantitatively address this issue, previous theories have suggested that certain types of phonons, *e.g.* acoustic phonons, participate in the nonresonant electronic energy transfers.[32,35]

**3.3.4 The relative importance.** Both mechanisms may simultaneously play roles in nonresonant intermolecular vibrational energy transfers in condensed phases. Which mechanism is more important, depends on the detailed situation. We expect that in liquid samples of relatively small energy gaps $\left(e.g.\ \frac{\Delta\omega}{\tau^{-1}} < 10\right)$ where well defined phonons are scarce and vibrational dephasings are generally fast, the energy transfer through the dephasing mechanism can be much faster than that through the phonon compensation mechanism. In crystalline samples with relatively large energy gaps $\left(e.g.\ \frac{\Delta\omega}{\tau^{-1}} > 10\right)$, vibrational dephasings are relatively slow, and many phonons with energy equal to the donor–acceptor gap may be available. Under the conditions, the energy transfer through the phonon compensation mechanism can be dominant. In glass, where the vibrational dephasing is relatively slow but the phonon density is not as large as that in the crystalline sample, either mechanism can be important.

# 4. Experimental results

## 4.1 Energy transfer systems and methods of rate measurements

The energy transfer systems we studied are KSCN/$KS^{13}CN$/$KS^{13}C^{15}N$ crystals and their aqueous and DMF solutions. In the samples, the vibrational energy of the nitrile stretch first excited state can resonantly and nonresonantly transfer between the three anions: $SCN^-$, $S^{13}CN^-$, and $S^{13}C^{15}N^-$. In the vibrational energy transfers the energy donor and acceptor are the nitrile stretch modes. In the crystalline samples at room temperature, the CN stretch 0–1 transition frequency of $SCN^-$ is 2051 $cm^{-1}$ with a (fit) Lorentzian line width 5.0 $cm^{-1}$, and those of $S^{13}CN^-$ and $S^{13}C^{15}N^-$ are 2003 $cm^{-1}$ and 1976 $cm^{-1}$ respectively (Fig. 1A and B). The line widths are the same for all three nitrile stretches. In DMF (Fig. 1C and D), the frequencies of the three nitrile stretches all blueshift for 6 $cm^{-1}$ but the gaps between any two remain the same, and the line widths increase to $\sim$7.0 $cm^{-1}$. In $D_2O$ (Fig. 1E and F), the nitrile frequencies blueshift by a larger amount $-15$ $cm^{-1}$ again with the same energy gaps, and the line widths broaden to 14 $cm^{-1}$.

In the three types of samples, the molecular environments are very different as partially indicated by the line width changes, but the energy gaps among the three nitrile stretches remain the same at the values of 48 $cm^{-1}$ (between $SCN^-$ and $S^{13}CN^-$) and 75 $cm^{-1}$ (between $SCN^-$ and $S^{13}C^{15}N^-$). Because the electronic properties including the nitrile stretch 0–1 transition dipole moments of the three anions are hardly affected by the isotope substitutions, measuring the vibrational energy transfers among them can explicitly reveal the donor–acceptor energy gap dependent energy transfer rates in different environments.

To measure the nitrile stretch resonant vibrational energy transfer of which the energy gap $\Delta\omega = 0$, we used the resonant energy transfer induced anisotropy decay method.[19,40,52] As shown in Fig. 2A (unnormalized data are provided in the ESI†), the signal anisotropy of the nitrile stretch ($^{13}C^{15}N$) 1st excited state decays with the increase of waiting time in saturated KSCN/$KSC^{13}C^{15}N$ $D_2O$ solutions with different KSCN/$KSC^{13}C^{15}N$ ratios.[19] In general, anisotropy decay is caused by two types of molecular dynamics: molecular rotations and resonant energy transfer from one molecule to another molecule with a different orientation. The nonresonant energy transfers between $SCN^-$ and $S^{13}C^{15}N^-$ are too slow (compared to the anisotropy dynamics) to make any significant contributions to the anisotropy decay.[19,40] When very few resonant acceptors are available, *e.g.* in the 1% or 2% samples, the resonant energy transfer is very slow, and the signal anisotropy decay is mainly caused by the rotations of the anion with a time constant of 10 $\pm$ 1 ps. With more resonant energy acceptors available (larger $KS^{13}C^{15}N$/KSCN ratios), the decay becomes faster. In the 100% sample, the anisotropy decays with a time constant 2.3 $\pm$ 0.2 ps. This fast decay is mainly the result of fast resonant energy transfer. From the two values, the resonant energy transfer time in the 100% sample is 3 ps (1/(1/2.3–1/10)). In the 50% sample (KSCN/$KS^{13}C^{15}N$ = 1/1), the resonant energy transfer time is 6 ps. As shown in Fig. 2B, the same method was also used to measure the resonant energy transfers of the nitrile stretch in the KSCN/$KSC^{13}C^{15}N$ mixed crystals at room temperature. The resonant energy transfer time constant in the pure crystal is 1.8 ps and that in the 1/1 mixed crystal is 3.6 ps.[40] The resonant energy transfers in other samples were measured using the same methods. A difference between the signal anisotropy decays in the liquid and solid samples is that the anisotropy values at long waiting times are zero in the liquid samples but nonzero in the solid samples. The reason is that in liquids the molecular rotations and orientations are completely randomized, but in the solids the rotations are hindered and the relative orientations of the molecules are not random which leads to a residual anisotropy. The residual anisotropy value was quantitatively calculated based on the hindered rotations and the relative molecular orientations in the crystals.[40] We also conducted experiments and verified that that the isotope substations in $S^{13}C^{15}N^-$ have negligible effects on the rotation and resonant energy transfer dynamics as the measured rotational and resonant energy transfer time constants are the same for both $SCN^-$ and $S^{13}C^{15}N$ anions.

To measure the nonresonant energy transfers of nitrile stretches between $SCN^-$ and $S^{13}CN^-$ with an energy donor–acceptor gap of 48 $cm^{-1}$ and between $SCN^-$ and $S^{13}C^{15}N^-$ with an energy donor–acceptor gap of 75 $cm^{-1}$, the vibrational energy exchange method[18,19] was used. Fig. 3A displays the waiting time dependent 2D IR spectra of a saturated KSCN/$KS^{13}C^{15}N$ = 1/1 $D_2O$ solution for which the FTIR spectrum is shown in Fig. 1F. At a very short waiting time, *e.g.* 0.2 ps, there

Published on 20 May 2014. Downloaded by Peking University on 9/2/2022 10:14:10 AM.

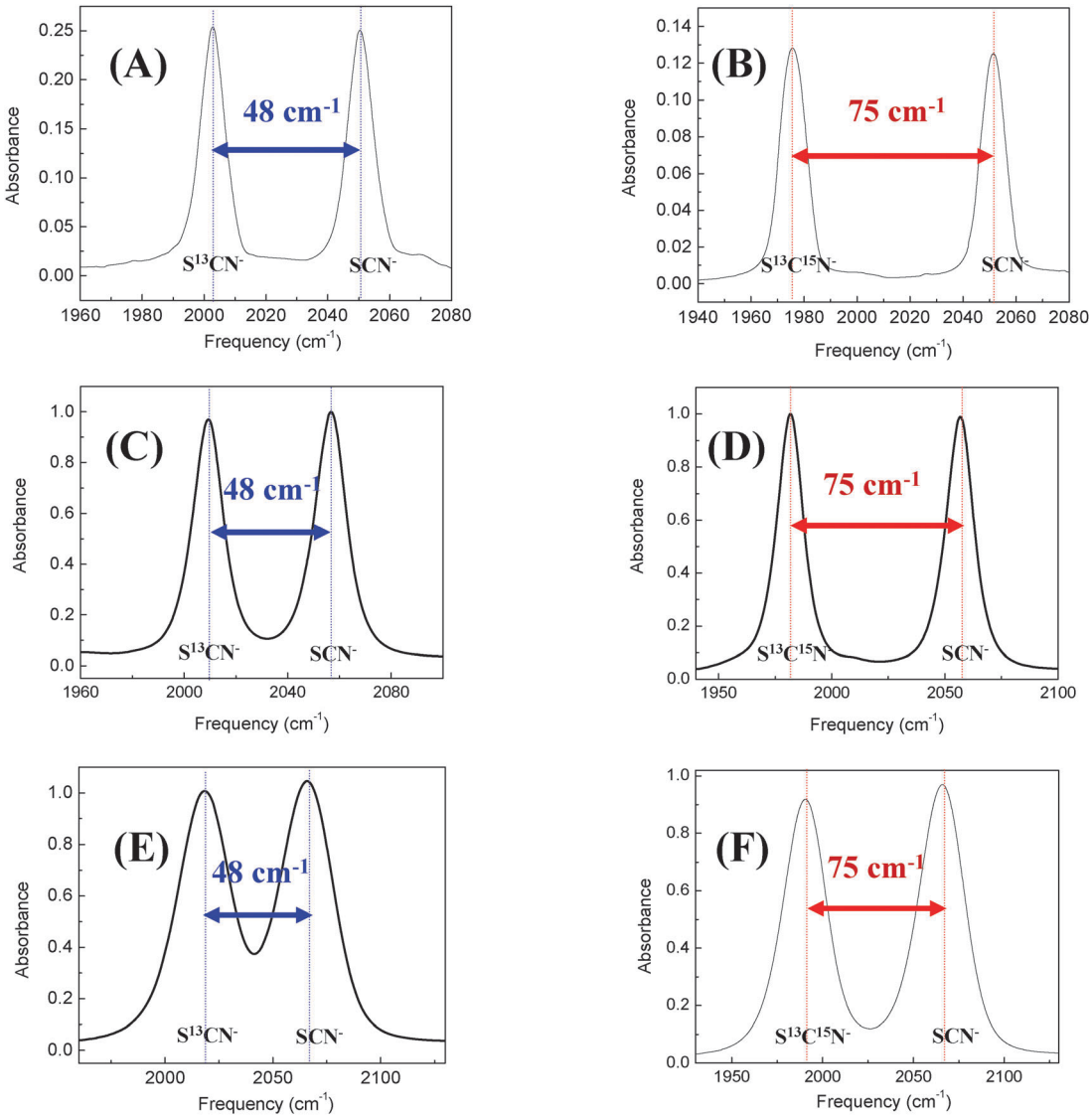


Fig. 1 FTIR spectra of KSCN/KS$^{13}$CN = 1/1 and KSCN/KS$^{13}$C$^{15}$N = 1/1 showing the nitrile stretch 0–1 transition peaks in (A) and (B) the crystalline samples, in (C) and (D) DMF (with a 1/8 salt/DMF molar ratio, ~1.6 M) saturated solutions, and in (E) and (F) $D_2O$ (10 M) saturated solutions at room temperature.

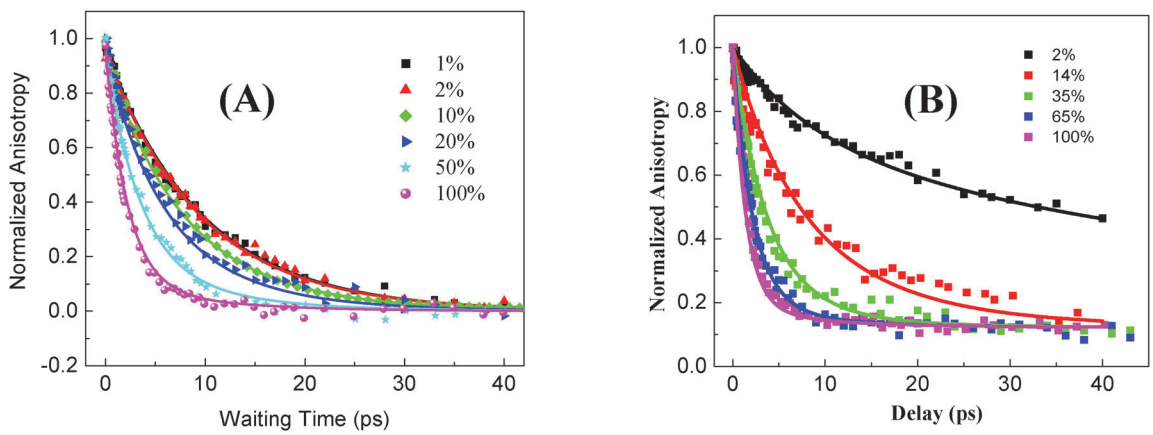


Fig. 2 Waiting time dependent anisotropy decays of the nitrile stretch vibrational excitation signal with different resonant energy acceptor ratios (by adjusting the ratio of KSCN/KS$^{13}$C$^{15}$N) of (A) KSCN/KS$^{13}$C$^{15}$N $D_2O$ saturated solutions (10 M), and (B) KSCN/KS$^{13}$C$^{15}$N mixed crystals at room temperature. Dots are data, and lines are kinetic model calculations.[19,40]

 This journal is © the Owner Societies 2014

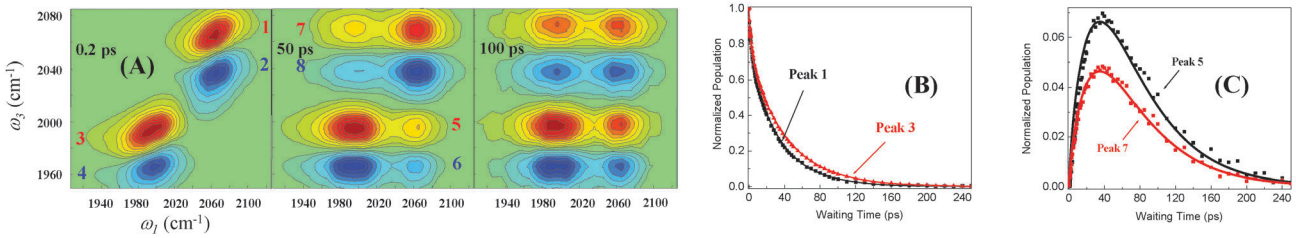


Fig. 3 (A) 2D IR spectra of a saturated (10 M) KSCN/KS$^{13}$C$^{15}$N = 1/1 $D_2O$ solution at room temperature at three waiting times; (B) and (C) the waiting time dependent intensities of peaks 1, 3, 5, 7 in (A). The parameters in the calculations of (B) and (C) were provided in our previous publication.[19]

Published on 20 May 2014. Downloaded by Peking University on 9/2/2022 10:14:10 AM.

are only two pairs of peaks on the diagonal positions in the spectrum. Peaks 1 and 2 are the CN stretching 0–1 and 1–2 transition peaks respectively, and peaks 3 and 4 are the corresponding transition peaks of the $^{13}C^{15}N$ stretch. With the increased waiting time, the vibrational excitations of both nitrile stretches begin to exchange, which produces two pairs of peaks (peaks 5–8) in the off-diagonal positions (panel 50 and 100 ps). Peaks 5 and 6 originate from the energy transfer from the CN stretching 1st excited state to that of the $^{13}C^{15}N$ stretch, and peaks 7 and 8 originate from the reverse energy transfer. From panels 50 ps and 100 ps, it can be seen that the peak amplitudes of 5 and 6 are larger than those of 7 and 8 for the same waiting time. This is because of the detailed balance principle: the down-flowing energy process must be faster than the up-energy process with a rate ratio determined almost exactly by the Boltzmann factor. Simultaneously analyzing the time dependent intensities of peaks 1, 3, 5, and 7 with the energy exchange kinetic model quantitatively gives the energy transfer time constants of both down-flowing $\left(\frac{1}{k_{CN\rightarrow{}^{13}C^{15}N}}\right)$ and up-pumping $\left(\frac{1}{k_{{}^{13}C^{15}N\rightarrow CN}}\right)$ processes to be $\frac{1}{k_{CN\rightarrow{}^{13}C^{15}N}} = 115 \pm 10$ ps, and $\frac{1}{k_{{}^{13}C^{15}N\rightarrow CN}} = 164 \pm 15$ ps (Fig. 3B and C).[19] Analyzing peaks 2, 4, 6, and 8 gives the same results.[19] The energy transfer rate ratio $\frac{k_{{}^{13}C^{15}N\rightarrow CN}}{k_{CN\rightarrow{}^{13}C^{15}N}}$ is determined to be 0.7, which is identical to the Boltzmann factor of the energy difference between the CN and $^{13}C^{15}N$ stretches $\left(e^{-\frac{\Delta\omega}{RT}} = e^{-\frac{75}{200}} = 0.7\right)$, verifying the prediction by the detailed balance principle in the energy transfer equations eqn (5), (24) and (25). Using the same method, the energy transfers between the two nitrile stretches in a KSCN/KS$^{13}$C$^{15}$N = 1/1 mixed crystal at room temperature were also measured. Data are provided in Section 4.5.

### 4.2 Vibrational energy transfers in aqueous solutions

The nonresonant and resonant vibrational energy transfers among the nitrile stretches in KSCN/KS$^{13}$CN/KS$^{13}$C$^{15}$N aqueous solutions of concentrations from 1 M to saturation at room temperature were previously measured by us.[18,19,40] Here we use these data to further analyze the energy transfer mechanism and molecular structures behind them. As reported[18] and discussed above, in a saturated KSCN/KS$^{13}$C$^{15}$N = 1/1 $D_2O$ solution, the nonresonant energy transfer time from the CN stretch to the $^{13}C^{15}N$ stretch with the energy gap $\Delta\omega$ = 75 cm$^{-1}$ is $\frac{1}{k_{CN\rightarrow{}^{13}C^{15}N}} = 115 \pm 15$ ps, and the resonant energy transfer time of the CN stretches with $\Delta\omega$ = 0 cm$^{-1}$ is $\frac{1}{k_{{}^{13}C^{15}N\rightarrow{}^{13}C^{15}N}} = \frac{1}{k_{CN\rightarrow CN}} = 6 \pm 0.6$ ps. In a saturated KSCN/KS$^{13}$CN = 1/1 $D_2O$ solution, the nonresonant energy transfer time from the CN stretch to the $^{13}$CN stretch with the energy gap of $\Delta\omega$ = 48 cm$^{-1}$ is $\frac{1}{k_{CN\rightarrow{}^{13}CN}} = 46 \pm 7$ ps. In other words, upon the energy gap increase from 0 to 48 cm$^{-1}$ to 75 cm$^{-1}$, the energy transfer time slows down from 6 ps to 46 ps to 115 ps. This large rate change can be seen by a simple inspection of the anisotropy decay curve and the 2D IR spectra in Fig. 4.

The energy transfer slows down by more than twofold when the energy gap increases from 48 cm$^{-1}$ to 75 cm$^{-1}$. As discussed in Section 3, either the dephasing mechanism or the phonon compensation mechanism can lead to energy gap dependent energy transfer rates. We first consider the phonon compensation mechanism. According to eqn (24), in order for the energy transfer rate with a gap 48 cm$^{-1}$ to be 2.5 times of that with a gap 75 cm$^{-1}$, the effective phonon density ratio at the two energy gaps needs to be $\frac{\rho_{eff}(75\ cm^{-1})}{\rho_{eff}(48\ cm^{-1})} = 1.7$. However, as discussed above, the effective phonon density involved in energy transfer cannot be experimentally measured. Only the relative amplitudes of system/phonon coupling strength $V_{ph}(s,q)$ inside $\rho_{eff}(\Delta E)$ can be estimated. The value of $V_{ph}(s,q)$ is mainly determined by the phonon modulation difference between the ground state and the first excited state of which the energy difference is about 2000 cm$^{-1}$ for both from CN to $^{13}$CN and from CN to $^{13}C^{15}N$ energy transfer processes. Because the chemical properties of these three nitrile stretches are essentially identical and the 1st excited state energy difference between $^{13}$CN and $^{13}C^{15}N$ is only 27 cm$^{-1}$ which is significantly smaller than the energy gap between the ground and first excited states. Therefore, the system/phonon coupling strengths in both nonresonant energy transfer processes are expected to be very similar if the phonon natures at both energy gaps are similar. We can also approximately estimate the relative amplitudes of phonon density ($\rho_s(\Delta E)$) from far IR (THz) or Raman or neutron scattering measurements. Fig. 5 displays (A) the room temperature THz absorption spectra of a KSCN crystalline sample (300 microns thick), a KSCN/$D_2O$ saturated solution sample

Published on 20 May 2014. Downloaded by Peking University on 9/2/2022 10:14:10 AM.

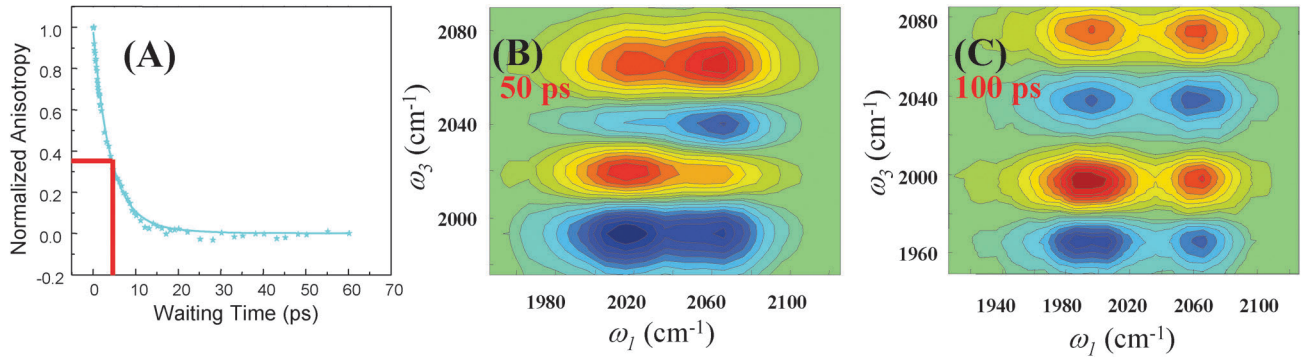


Fig. 4 (A) The $^{13}C^{15}N$ stretch 1st excited state excitation signal anisotropy decay curve (blue) of a saturated KSCN/$KS^{13}C^{15}N$ = 1/1 $D_2O$ solution. The red lines indicate roughly where the decay time constant is. (B) The 2D IR spectrum of a saturated KSCN/$KS^{13}CN$ = 1/1 $D_2O$ solution at a waiting time 50 ps. The similar intensities of corresponding diagonal and cross peaks along the *y*-axis indicate that the energy transfer time constant is around 50 ps. (C) The 2D IR spectrum of a saturated KSCN/$KS^{13}C^{15}N$ = 1/1 $D_2O$ solution at a waiting time 100 ps. The similar intensities of corresponding diagonal and cross peaks along the *y*-axis indicate that the energy transfer time constant is around 100 ps. The detailed quantitative energy transfer time constants are obtained from rigorous kinetic model calculations.[18,19]

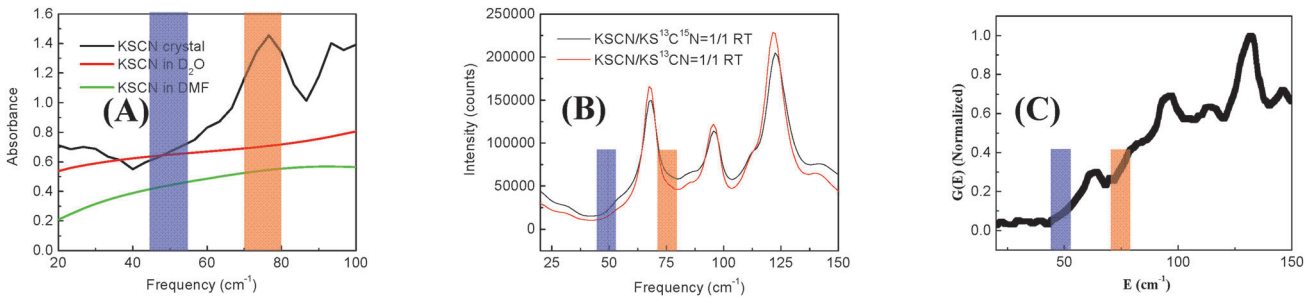


Fig. 5 (A) The room temperature THz absorption spectra of a KSCN crystalline sample (300 microns thick), a KSCN/$D_2O$ saturated solution sample (about 0.5–3 microns thick), and a KSCN/DMF saturated solution (0.5–3 microns thick); (B) the room temperature Raman spectra of KSCN/$KS^{13}C^{15}N$ = 1/1 and KSCN/$KS^{13}CN$ = 1/1 crystalline samples. The results show that the isotope labeling doesn't change the phonon modes; and (C) the neutron scattering data of crystalline KSCN at 10 K in the frequency range of 20–100 cm$^{-1}$. The neutron scattering data are obtained from literature.[53] The two semitransparent columns indicate the two energy gaps 48 cm$^{-1}$ and 75 cm$^{-1}$.

(about 0.5–3 micron thick), and a KSCN/DMF saturated solution (0.5–3 micron thick); (B) the room temperature Raman spectra of KSCN/$KS^{13}C^{15}N$ = 1/1 and KSCN/$KS^{13}CN$ = 1/1 crystalline samples; and (C) the neutron scattering data of crystalline KSCN at 10 K in the frequency range of the two energy gaps.[53] In the $D_2O$ and DMF KSCN solutions, the absorbance from 40 cm$^{-1}$ to 80 cm$^{-1}$ increases slightly in a continuous way. These are the absorption of the solvents. In the KSCN crystal, there is an absorption peak at 70–75 cm$^{-1}$. This peak appears in all the three different types of measurements. If we assume that $\rho_s(\Delta E)$ is proportional to the absorption coefficient which can be obtained from the solution spectra is Fig. 5A, the calculated energy transfer rate ratio at the two energy gaps (48 and 75 cm$^{-1}$) based on eqn (24) is consistent with the measured rate ratio. However, as measured, the energy transfer rates with the energy gap 75 cm$^{-1}$ in both $D_2O$ solution and crystal are about the same, and the vibrational couplings in both samples are also very similar.[40] $\rho_s(\Delta E)$ and therefore the absorption coefficient should be very similar in both samples (based on the assumption) if the energy transfers in both samples are through the phonon compensation mechanism. This is very different from the absorption measurements in Fig. 5A that the absorption coefficient of KSCN crystal is about 100 times smaller than those of $D_2O$ or DMF in the frequency range. The result suggests that either the assumption that $\rho_s(\Delta E)$ is proportional to the absorption coefficient or the phonon/system coupling is constant is invalid or the energy transfer is not through the phonon compensation mechanism. If the assumption is invalid (our results in solids to be discussed do strongly suggest that there is some strong connection between the optical spectral density and $\rho_s(\Delta E)$), the phonon compensation mechanism can still be conceivable but another way yet to be developed, is needed to test it. If the phonon compensation mechanism is invalid, the energy transfer can go through the other mechanism – the dephasing mechanism.

If the energy transfers are through the dephasing mechanism, eqn (5) must be able to describe both the resonant energy transfer and the two nonresonant energy transfers with the same parameters. From experiments ($T$ = 295 K), we know three energy transfer time constants $1/k$ = 6, 46, and 115 ps from energy transfers with three energy gaps $\Delta\omega$ = 0, 48, and 75 cm$^{-1}$. Eqn (5) has only two unknown parameters ($V$ and $\tau$), and we have three sets of data which guarantee single values for the two parameters. Substituting the energy transfer rate constants and energy gaps into eqn (5), we obtain $V$ = 4.1 cm$^{-1}$ and $\tau^{-1}$ = 15 cm$^{-1}$. With these two constants,

 This journal is © the Owner Societies 2014

Published on 20 May 2014. Downloaded by Peking University on 9/2/2022 10:14:10 AM.

the calculated energy transfer time constants are 6.1 ps ($\Delta\omega$ = 0), 49 ps ($\Delta\omega$ = 48 $cm^{-1}$) and 105 ps ($\Delta\omega$ = 75 $cm^{-1}$). These values are the same as those experimental results within experimental uncertainty. Here one issue needs to be emphasized. In converting the dephasing time $\tau$ with the line width ($\tau^{-1}$) in the denominator of eqn (5), a factor of $2\pi$ is needed, *e.g.* if $\tau^{-1}$ = 15 $cm^{-1}$, $\tau$ must be $\tau = \frac{1}{2\pi}\frac{100}{15\times 3}$ ps = 0.35 ps.

Now, we need to evaluate whether the two obtained parameters $V$ = 4.1 $cm^{-1}$ and $\tau^{-1}$ = 15 $cm^{-1}$ are in reasonable ranges. As discussed in Section 3, the energy transfer dephasing line width ($\tau^{-1}$) must not be larger than the sum of the donor and acceptor 0–1 transition line widths. As determined in Fig. 1E and F, the nitrile stretch line width in the saturated $D_2O$ solution is 14 $cm^{-1}$. The line width sum of the energy donor and acceptor is therefore 28 $cm^{-1}$. The determined energy transfer line width $\tau^{-1}$ = 15 $cm^{-1}$ is about 50% of the sum, indicating that the dephasings of the donor and acceptor are correlated.

To evaluate the coupling strength $V$ = 4.1 $cm^{-1}$, we need to know the structures of the aqueous solutions. As we reported previously with many control experiments, ions in concentrated KSCN aqueous solutions contain a large fraction of ion clusters.[19–22,54] The measured energy transfers in the saturated $D_2O$ solutions are the sum of energy transfers from one donor to many acceptors that are various distances away from the donor. In our previous treatment,[18,19] we averaged the energy transfer rate over the effective acceptors and based on this averaged rate a number of the effective energy acceptors was obtained, *e.g.* in the saturated KSCN/$KS^{13}C^{15}N$ = 1/1 $D_2O$ solution the effective energy acceptor number is 9. Using 9 as the acceptor number, the coupling strength between one donor and one acceptor can be obtained to be $V_{1\to 1} = \frac{V}{\sqrt{9}} = \frac{4.1}{3} = 1.4$ $cm^{-1}$. Now we can use the transition dipole–transition dipole interaction equation eqn (26) to calculate the average donor–acceptor distance based on $V_{1\to 1}$ = 1.4 $cm^{-1}$. We have the parameters from the literature[19] to be $n$ = 1.5, $\mu_D = \mu_A$ = 0.33D, $\langle\kappa\rangle = \sqrt{2/3}$ (randomized, because the rotation of anion is faster than the energy transfer). The donor–acceptor distance $r_{DA}$ is calculated to be $r_{DA}$ = 5.1 Å. This value is larger than the shortest anion distance (4.0 angstroms) in the KSCN crystal but is smaller than the nominal anion distance (5.6 angstroms) if ion clustering does not occur.[40] If we assume that the ion packing patterns are somewhat similar in the cluster and the crystal, the obtained $r_{DA}$ = 5.1 Å value is very reasonable. In the KSCN crystal[40] surrounding one anion, there are four closest anions at a distance of 4.0 angstroms. The next two anions are at distances of 4.8 angstroms, and then two at 5.6 angstroms, and two at 6.2 angstroms. The 17 and 18 anions are at a distance of 6.7 angstroms. The obtained average distance is larger than when using the first three acceptors (each type of anions divided by 2 as the sample is KSCN/$KS^{13}C^{15}N$ = 1/1) but smaller than when the remaining six are also included. We can use another method to estimate the energy donor–acceptor distance based on $V$ = 4.1 $cm^{-1}$. If we assume that the ion packing patterns are somewhat similar in the cluster and the crystal, in other words, the number of anions in each layer of anions surrounding any one anion is the same in both the cluster and crystal but in the crystal the anions have certain orientations and in the crystal the anions have random orientations, the energy transfer measured in the KSCN/$KS^{13}C^{15}N$ = 1/1 aqueous solution is mainly contributed from the transfers of one donor to the two closest anions because $\frac{1}{k_{DA}} \approx\propto r_{DA}^6$. Therefore, for this case the one donor to one acceptor coupling strength $V_{1\to 1}$ is $V_{1\to 1} = \frac{V}{\sqrt{2}} = 2.9$ $cm^{-1}$. This coupling strength gives a donor–acceptor distance of 4.0 angstroms, the same as in that in the crystal. However, in the saturated solutions, the ion clusters are large and contain many ions. The energy transfer rate measured is not simply the sum of transfers from one donor to many acceptors, but more like a chain reaction. In other words, the energy may transfer from the donor to an acceptor and from this acceptor to another anion, and so on, similar to those in the KSCN crystal.[40] Obviously, the above estimated donor–acceptor distances are only approximate.

To more precisely evaluate the coupling strength based on the donor–acceptor distance, what is needed is some ion clusters that contain fewer than five anions. Because in such small clusters the anions can form a structure of four anions surrounding one with a same distance as that in the crystal, the anion distance must be close to the shortest distance 4.0 angstroms in the crystal and no chain transfers need to be considered. This is experimentally achievable. As required by chemical equilibrium, in a more dilute KSCN solution, the ion clusters must become smaller and fewer. This was experimentally observed.[19] We previously determined that in the 1 M aqueous solutions, more than 25% of the ions form clusters and on average the clusters contain 3 $SCN^-$ anions.[19,40] In the 1 M KSCN/$KS^{13}C^{15}N$ = 1/1 solution, the energy transfer times are $\frac{1}{k_{CN\to {}^{13}C^{15}N}} = 180\pm 20$ ps ($\Delta\omega$ = 75 $cm^{-1}$), and $\frac{1}{k_{{}^{13}C^{15}N\to {}^{13}C^{15}N}} = \frac{1}{k_{CN\to CN}} = 10\pm 1$ ps ($\Delta\omega$ = 0).[40] Substituting these values into eqn (5), we obtain $V$ = 3.1 $cm^{-1}$ and $\tau^{-1}$ = 15.5 $cm^{-1}$. The one donor to one acceptor coupling strength is therefore $V_{1\to 1} = \frac{3.1}{\sqrt{1.5}} = 2.5$ $cm^{-1}$. Based on the coupling strength and eqn (24) and the above parameters, the donor–acceptor distance $r_{DA}$ in the cluster containing three anions is determined to be 4.3 angstroms, close to the closest anion distance of 4.0 angstroms in the crystal. Including all experimental uncertainties of each parameter, we estimate the uncertainty of the determined distance to be about 10% to 20%. The results indicate that eqn (5) of the dephasing mechanism describes the vibrational energy transfers of the KSCN/$KS^{13}CN$/$KS^{13}C^{15}N$ aqueous solutions very well.

The above discussion also resolves an issue that has puzzled us for the last two years. We previously observed that on average one-donor-to-one-acceptor resonant energy transfer is faster in a more dilute KSCN aqueous solution, and we speculated that it was because the ions were closer in a smaller cluster.[19] Here we use the previous energy transfer results and eqn (5) to derive

Published on 20 May 2014. Downloaded by Peking University on 9/2/2022 10:14:10 AM.

Table 1 The energy donor–acceptor distances in KSCN/$KS^{13}C^{15}N$ $D_2O$ solutions with different concentrations determined by the measured energy transfer rates and the number of ions in a cluster and eqn (5). Other parameters in the calculations are $n$ = 1.5, $\mu_D = \mu_A$ = 0.33 D, $\langle\kappa\rangle = \sqrt{2/3}$

| | 10 M | 8.8 M | 6.5 M | 4 M | 1.8 M | 1 M |
|---|---|---|---|---|---|---|
| $\frac{1}{k_{CN\rightarrow CN}}$(ps) | 6.0 | 6.2 | 7.1 | 10 | 9 | 10 |
| $\frac{1}{k_{CN\rightarrow {}^{13}C^{15}N}}$(ps) | 115 | 110 | 130 | 140 | 160 | 180 |
| $n$ (# of anions in cluster) | 18 | 13 | 9 | 5 | 4 | 3 |
| $\tau^{-1}$ ($cm^{-1}$) | 15.0 | 15.0 | 15.0 | 18.0 | 15.5 | 15.5 |
| $V_{1\rightarrow 1}$ ($cm^{-1}$) | 1.4 | 1.57 | 1.74 | 2.06 | 2.34 | 2.53 |
| $r_{DA}$ (Å) | 5.1 | 5.0 | 4.8 | 4.6 | 4.4 | 4.3 |

the average donor–acceptor distances in the ion clusters of the KSCN aqueous solutions of different concentrations. The results are listed in Table 1. As we can see from Table 1, the energy donor–acceptor average distance is largest (5.1 Å) in the saturated solution (10 M). It gradually becomes smaller with the decrease of ion concentration in the solutions. In the 1 M solution, the distance is 4.3 Å, very close to that of the shortest distance in the KSCN crystal. We believe that the donor–acceptor distance change does not reflect the ion distance change in the ion clusters. Instead, the distance change is more because in the more concentrated solutions, the ion clusters have more ions so that the energy acceptors have to distribute around the energy donor with different distances. The measured energy transfer is the sum of transfers from the donor to all acceptors and the chain transfers from the initial acceptors to the secondary and tertiary acceptors and so on. The result of the chain transfer is that the average donor–acceptor distance is larger than the shortest anion–anion distance. Only in dilute solutions, the ion clusters are sufficiently small so that all energy acceptors can be at the same distance to the donor as constrained by the space available. In such solutions, the average donor–acceptor distance is the same as the anion distance in the cluster. Assuming that the crystalline structure applies, surrounding an $SCN^-$ anion, the first solvation shell of a distance 4 Å can contain four $SCN^-$ anions. We expect that in the ion clusters the first solvation of any anion can also contain at most four anions. Because of this restriction, in the 1 M and 1.8 M solutions where the ion clusters contain 3 and 4 anions the energy donor–acceptor distances are very close to 4 Å. The determined distance 4.3 Å also suggests that the ion clusters are direct contact clusters.

In summary, eqn (5) of the dephasing mechanism and the transition dipole–transition dipole interaction eqn (26) quantitatively describe both resonant and nonresonant vibrational energy transfers in the KSCN/$KS^{13}CN$/$KS^{13}C^{15}N$ $D_2O$ solutions very well. However, the anion distances in the ion clusters are difficult to determine using other experimental techniques. A system with a well-defined donor–acceptor distance that can be determined by some mature techniques, *e.g.* XRD, is highly desired to benchmark the method. We recently made a significant step towards this goal by directly measuring the resonant energy transfers among the $SCN^-$ anions in the KSCN crystal. Using eqn (5) and (26), the shortest anion distance determined from the experimental energy transfer time constant is 3.9 ± 0.3 Å, identical to that (4 Å) determined using XRD.[40]

### 4.3 Temperature dependent vibrational energy transfers in aqueous solutions

One of the interesting predictions of eqn (5) is that the resonant energy transfer will become slower and the nonresonant energy transfer will become faster at a higher temperature if $\Delta\omega > \tau^{-1} > V$ (for $\Delta\omega \neq 0$) and $\tau^{-1} > V$ (for $\Delta\omega = 0$) and no chemical transformations occur within the temperature range, because at a higher temperature molecular motions are faster and the energy transfer dephasing caused by the motions typically becomes faster accordingly ($\tau^{-1}$ is larger at a higher temperature). The faster energy transfer dephasing may be because of faster donor–acceptor dephasings and/or because the dephasings of donor and acceptor are less correlated. Measurements of the resonant and nonresonant vibrational energy transfers in the KSCN/$KS^{13}C^{15}N$ $D_2O$ 10 M solutions from room temperature to 80 °C fulfill the requirements. As described above, at room temperature, the resonant energy transfer among the nitrile stretches in the KSCN/$KS^{13}C^{15}N$ = 1/1 $D_2O$ 10 M solutions have a time constant of 6 ps, and the nonresonant energy transfer from $SCN^-$ to $S^{13}C^{15}N^-$ with an energy gap 75 $cm^{-1}$ has a time constant of 115 ps. As shown in Fig. 6, at 80 °C, the resonant energy transfer time slows down to 6.8 ps $\left(2\Big/\left(\frac{1}{1.7}-\frac{1}{3.4}\right)=6.8\right)$ from 6 ps at room temperature, but that of the nonresonant energy transfer becomes faster, up to 95 ps from 115 ps. The observed opposite temperature dependences of resonant and nonresonant energy transfers are consistent with the prediction by eqn (5). Substituting the two values into eqn (5), we obtain $V$ = 4.1 $cm^{-1}$ and $\tau^{-1}$ = 17.5 $cm^{-1}$ with a calculated resonant transfer time of 6.7 ps and the nonresonant time 94 ps at 80 °C. The coupling strength (4.1 $cm^{-1}$) is the same as that at room temperature, but the dephasing line width (17.5 $cm^{-1}$) is larger than that at room temperature. The same coupling strength indicates that the average anion distance at 80 °C is similar to that at room temperature in the same solution, because the other parameters in equation eqn (26) which correlate the coupling strength with the distance are weakly temperature dependent. This is consistent with the temperature dependent FTIR measurements (in ESI†). The larger energy transfer dephasing line width indicates that the energy transfer dephasing at 80 °C is faster. As discussed, this is probably because the molecular motions are faster. This is supported by the faster molecular rotation at 80 °C (3.4 ps) compared to that at room temperature (10 ps).

### 4.4 Resonant and nonresonant energy transfers in DMF solutions

The energy-gap dependence of vibrational energy transfers in the $D_2O$ solutions described above is also observed in KSCN/$KS^{13}CN$/$KS^{13}C^{15}N$ DMF solutions with a salt/DMF ratio 1/8,

 This journal is © the Owner Societies 2014

Published on 20 May 2014. Downloaded by Peking University on 9/2/2022 10:14:10 AM.

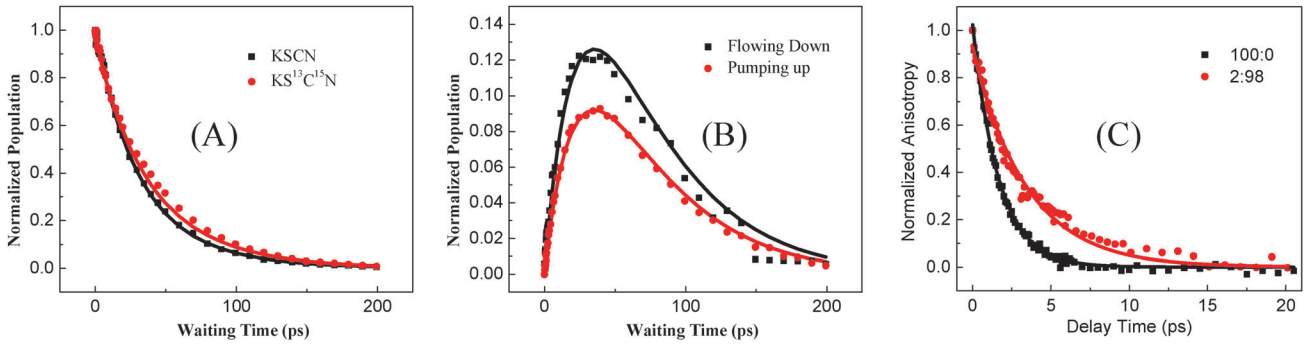


Fig. 6 (A) and (B) are the intensities of 1–2 transition peaks (similar to peaks 2, 4, 6, 8 in Fig. 3) of 10 M KSCN/$KS^{13}C^{15}N$ = 1/1 $D_2O$ solutions at 80 °C. Dots are data and curves are kinetic model calculations. (C) Anisotropy decays of the nitrile stretch first excited state with 2% resonant energy acceptor (red) and with 100% resonant acceptor in 10 M KSCN/$KS^{13}C^{15}N$ $D_2O$ solutions at 80 °C. Dots are data and curves are fits with single exponentials with time constant 3.4 ps (red) and 1.7 ps (black).

though the molecular properties and intermolecular interactions in the $D_2O$ and DMF solutions are very different.

We also used the anisotropy decay method to measure the resonant energy transfer rate among the $SCN^-$ anions in the 1/8 KSCN/DMF solution. As displayed in Fig. 7A, different from that in the $D_2O$ solutions, the anisotropy decays of the CN stretch of the pure KSCN and the $^{13}C^{15}N$ stretch of the 5/95 sample in the 1/8 solutions are not single exponential. They exhibit a clear biexponential behavior: a fast component with a weighting factor of ~44% and a time constant of 3.4 ps and a slow component with a weighting factor of 56% with a time constant of 13.7 ps (100% KSCN solution) and 30.7 ps ($KS^{13}C^{15}N$/KSCN = 5/95) respectively. In a very dilute (1 wt%) KSCN DMF solution, the anisotropy decay of CN excitation is a single exponential

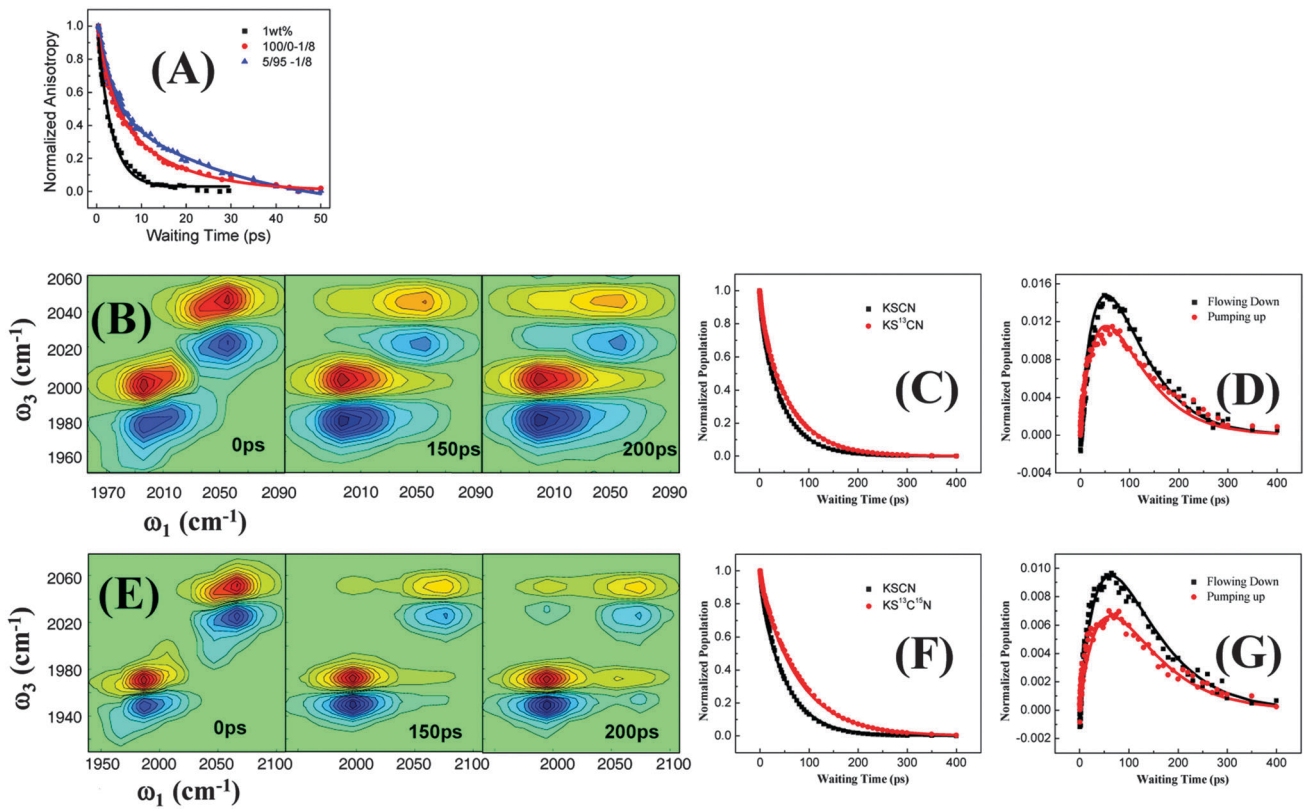


Fig. 7 (A) Anisotropy decay data of CN stretch 1st excited state of 1 wt% KSCN in DMF (black), a KSCN/DMF solution with a 1/8 molar ratio (~1.6 M), and of $^{13}C^{15}N$ stretch 1st excited state of a $KS^{13}C^{15}N$/KSCN = 5/95 DMF solution with a 1/8 salt/DMF molar ratio. Dots are data, and lines are single exponential fit (black) with and biexponential fits (red & blue).[17] (B) Waiting time dependent 2D IR spectra of a KSCN/$KS^{13}CN$ = 1/1 DMF solution with a 1/8 salt molar ratio (~1.6 M). (C) and (D) The time dependent diagonal and cross blue peak intensities of (B). Dots data and curves are kinetic model calculations. (E) Waiting time dependent 2D IR spectra of a KSCN/$KS^{13}C^{15}N$ = 1/1 DMF solution with a 1/8 salt molar ratio. (F) and (G) The time dependent diagonal and cross blue peak intensities of (E). Dots are data and curves are kinetic model calculations.

Published on 20 May 2014. Downloaded by Peking University on 9/2/2022 10:14:10 AM.

with a time constant of 3.1 ps (black in Fig. 7A), which is the rotational time constant of the free anions as in such a dilute solution most ions are expected to be separated by the DMF solvent molecules. Similar to the $D_2O$ solutions, KSCN ions in the concentrated 1/8 DMF solutions are expected to form some ion clusters. We suspect that the fast decay component of the 1/8 samples is because of the rotation of the free anions in the solutions, as the time constant (3.4 ps) is very similar to that of the free anion in the dilute solution (3.1 ps), and the slow component is because of the rotation and the resonant energy transfer of the ion clusters. With such an assumption, the ion cluster ratio in the 1/8 solution is the weighting factor of the slow component, 56%. The number of the anions in the cluster can be estimated to be around 4–6 from the rotational time ratio between the clustered and free anions (30.7/3.4–9) and the estimated relative volume ratio of the anion/cation. More discussion on the analysis is provided in ESI.† The resonant energy transfer time in the pure KSCN 1/8 solution can be obtained from the rate difference between the 100% and 5/95 1/8 samples (1/(1/13.7–1/30.7)) to be 24.7 ps, which indicates that the resonant energy transfer time constant in the KSCN/$KS^{13}C^{15}N$ = 1/1 1/8 DMF solution would be 24.7 × 2 = 49.4 ps as the number of acceptors is 50% fewer. Based on the cluster ratio 56% and 2D IR energy exchange measurements (Fig. 7B–G), the vibrational energy transfer time constant from CN to $^{13}CN$ in a KSCN/$KS^{13}CN$ = 1/1 1/8 DMF solution is determined to be 570 ps, and that from CN to $^{13}C^{15}N$ in a KSCN/$KS^{13}C^{15}N$ = 1/1 1/8 DMF solution is determined to be 1150 ps. Substituting the three time constants 49.4 ps ($\Delta\omega$ = 0), 570 ps ($\Delta\omega$ = 48 $cm^{-1}$) and 1150 ps ($\Delta\omega$ = 75 $cm^{-1}$) into eqn (5), we obtain the coupling strength $V$ = 1.25 $cm^{-1}$ and the dephasing width $\tau^{-1}$ = 14 $cm^{-1}$ with the calculated time constants 49 ps ($\Delta\omega$ = 0), 542 ps ($\Delta\omega$ = 48 $cm^{-1}$) and 1191 ps ($\Delta\omega$ = 75 $cm^{-1}$). The dephasing width is the sum of the donor–acceptor 0–1 transition line widths. Based on $V$ = 1.25 $cm^{-1}$ and the estimated anion number in the cluster (4–6) and eqn (26), the distance between two anions in an ion cluster in the 1/8 DMF solution is 5.3 Å (the transition dipole moment in DMF is about 27% smaller than that in $D_2O$). This value is about 20% larger than the shortest anion distance 4.0 Å in the KSCN crystal but significantly smaller than the average anion distance ~1 nm in the DMF solution if ions did not form clusters. The analysis shows that the vibrational energy transfers in the DMF solutions with three different donor–acceptor energy gaps can be simultaneously described reasonably well by eqn (5).

Summarizing the results in the KSCN/$KS^{13}CN$/$KS^{13}C^{15}N$ $D_2O$ and DMF solutions, we conclude that eqn (5) of the dephasing mechanism and eqn (26) of the transition dipole–transition dipole interaction describe the intermolecular vibrational energy kinetics and the correlation between the donor–acceptor distance and coupling in the solution very well. However, the experimental results do not provide strong evidence to support or object to eqn (24) and (25) of the phonon compensation mechanism of the second order perturbation approach, though comparing the results in the $D_2O$ and DMF solutions could provide some indirect hint against the phonon compensation mechanism. $D_2O$ and DMF are very different molecules. One would expect that the phonon densities (though the THz absorption patterns in the range of 30–100 $cm^{-1}$ are similar in Fig. 5A) and the phonon–anion interactions in the two solutions should be very different. If eqn (24) and (25) work, the energy donor–acceptor gap dependences of energy transfers in the two solutions are expected to be very different. This prediction is different from the experimentally observed similar gap dependence. The results seem to provide some evidence that is not easy to explain using the previous phonon compensation mechanism based on the first order perturbation:[15] in both samples, the energy transfer rate is inversely proportional to the square of the energy gap. In order to explain such an observation, the previous theory needs to assume the product of the phonon/system coupling and the phonon density at 48 $cm^{-1}$ is about 1.5 times of that at 75 $cm^{-1}$ at room temperature which seems to not be supported by the estimations in the literature.[4,15]

### 4.5 Vibrational energy transfers in crystals at room temperature

The benchmarking test of eqn (5) and (26) comes from the resonant energy transfer measurements (Fig. 2B) in KSCN/$KS^{13}C^{15}N$ crystals of which the energy donor–acceptor (anions) distances[40] have been well characterized with XRD and neutron diffraction methods.[53,55] The closest anion distance in the KSCN crystal is determined to be 3.9 ± 0.3 Å from the measured resonant energy transfer time constant and eqn (5) and (26). This value is the same as 4.0 Å that is determined by XRD. However, the nonresonant energy transfer results in the crystals are very surprising. They do not follow the observed energy gap dependence in the liquid samples described above. As shown in Fig. 8A and D, the vibrational energy exchange cross-peaks of the KSCN/$KS^{13}CN$ = 1/1 crystalline sample (Fig. 8A) is only slightly larger than those of the KSCN/$KS^{13}C^{15}N$ = 1/1 crystalline sample at the same waiting times at room temperature. The results indicate that the vibrational energy transfer from CN to $^{13}CN$ is only slightly faster than that from CN to $^{13}C^{15}N$. Quantitative analyses in Fig. 8B, C, E and F show that the energy transfer time from CN to $^{13}CN$ with an energy gap 48 $cm^{-1}$ is $\frac{1}{k_{CN\rightarrow{}^{13}CN}} = 96 \pm 5$ ps, and that from CN to $^{13}C^{15}N$ with a gap 75 $cm^{-1}$ is $\frac{1}{k_{CN\rightarrow{}^{13}C^{15}N}} = 99 \pm 5$ ps. This observed energy gap independence cannot be explained using eqn (5) of the dephasing mechanism.

As discussed in Section 3, both the dephasing mechanism and the phonon compensation mechanism play roles in non-resonant energy transfers, and depending on the detailed situation, one mechanism may dominate over the other. The nonresonant energy transfer data in Fig. 8 seem to suggest that the phonon compensation mechanism is dominant in the crystalline samples. To further explore this issue, we first use eqn (5) to estimate how fast the nonresonant energy transfers of the dephasing mechanism can be in the two crystalline samples. According to the resonant energy transfer time 3.6 ps and the average coupling strength 3.5 $cm^{-1}$ in the 1/1 mixed crystalline samples and eqn (5) (the resonant energy transfer rate needs to

 This journal is © the Owner Societies 2014

Published on 20 May 2014. Downloaded by Peking University on 9/2/2022 10:14:10 AM.

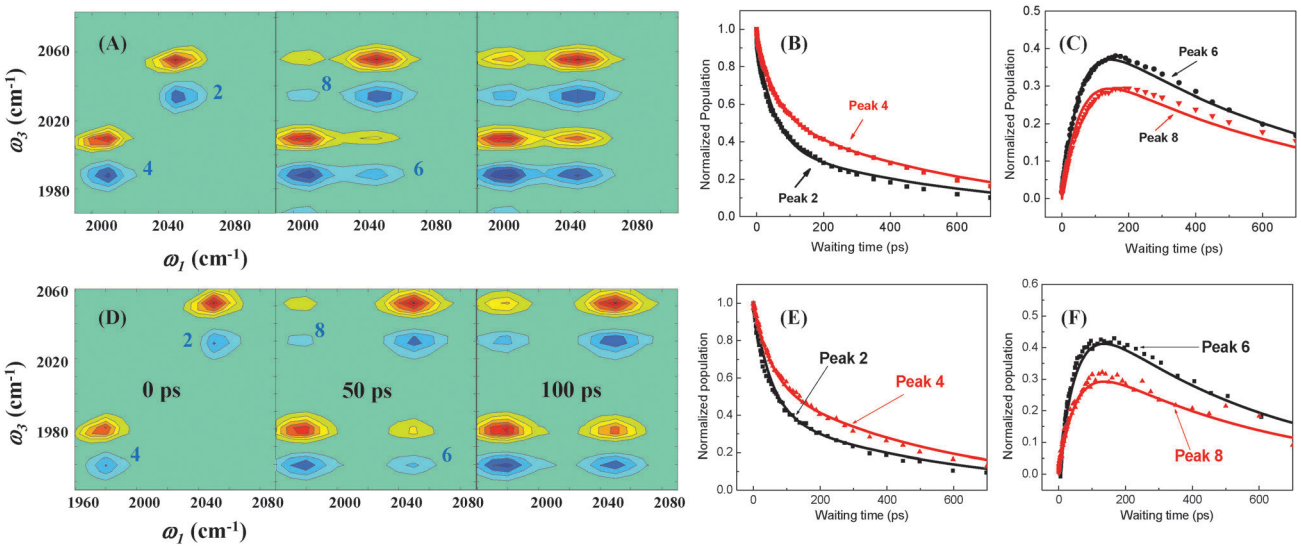


Fig. 8 (A) 2D IR spectra of a KSCN/KS$^{13}$CN = 1/1 mixed crystal at room temperature at three waiting times; (B) and (C) the waiting time dependent intensities of peaks 2, 4, 6, 8 in (A). Dots are experimental results, and lines are kinetic model calculations. (D) 2D IR spectra of a KSCN/KS$^{13}$C$^{15}$N = 1/1 mixed crystal at room temperature at three waiting times; (E) and (F) the waiting time dependent intensities of peaks 2, 4, 6, 8 in (D).

be calculated for each donor–acceptor pair[40]), the energy transfer dephasing line width ($\tau^{-1}$) is determined to be 8 cm$^{-1}$.[40] Based on the two parameters and eqn (5), the energy transfer time for an energy gap 48 cm$^{-1}$ is calculated to be $\frac{1}{k_{CN\rightarrow{}^{13}CN}} = 117$ ps and that for an energy gap 75 cm$^{-1}$ is calculated to be $\frac{1}{k_{CN\rightarrow{}^{13}C^{15}N}} = 262$ ps. However, we notice that in the KSCN crystals, the energy transfer dephasing width 8 cm$^{-1}$ is close to two times (4.6 cm$^{-1}$) the largest coupling between two adjacent anions. Under such a situation, eqn (5) is not very sensitive to $\tau^{-1}$ for the resonant energy transfer. $\tau^{-1}$ can vary from 3 cm$^{-1}$ to 8 cm$^{-1}$. This suggests that the actual energy transfer times predicted by eqn (5) can be even longer than these two values. Therefore, the two calculated values suggest that the experimentally observed $\frac{1}{k_{CN\rightarrow{}^{13}C^{15}N}} = 99$ ps must be mainly from the phonon compensation mechanism, and the experimental $\frac{1}{k_{CN\rightarrow{}^{13}CN}} =$ 96 ps can be dominated by either mechanism depending on the energy transfer dephasing time. If the dephasing mechanism is not considered, the observed energy gap independence can be qualitatively explained with eqn (24) and (25). If the phonon/system coupling strengths are the same at two energy gaps as discussed above, and the phonon density at 75 cm$^{-1}$ should be $\left(\frac{75}{48}\right)^2 \times \frac{[\exp(48/200)-1]^{-1}+1}{[\exp(75/200)-1]^{-1}+1} = 3.6$ times of that at 48 cm$^{-1}$, the experimental observations can be predicted by eqn (24). It is very interesting to see that all THz absorption, Raman and neutron scattering measurements (Fig. 5) do show that the peak density at ~75 cm$^{-1}$ is at least two times larger than that at 48 cm$^{-1}$. In the THz absorption spectrum, the peak ratio is about 2.2 times. In the Raman spectrum, the ratio is ~7.3 times. The neutron scattering experiments also show that the optical phonon densities at 75 cm$^{-1}$ are significantly larger than those at 48 cm$^{-1}$ (the ratio is estimated to be more than 5 from the literature).[56] The results seem to suggest that if optical phonons are the major phonons participating in the energy transfer process, the phonon densities at 75 cm$^{-1}$ must be at least a few times larger than those at 48 cm$^{-1}$. Another possible explanation for the two observed similar nonresonant energy transfer times is that the energy transfers must be energy gap independent if acoustic phonons with Debye approximation are assumed.[32] However, this later explanation is not supported by our temperature dependent experiments to be described in later paragraphs. The observed energy gap independence could also be explained by the phonon compensation mechanism of the first order approach if the product of the system/phonon coupling strengths and the phonon densities at 75 cm$^{-1}$ are 1.5 times those at 48 cm$^{-1}$. However, if the phonons involved in the transfer are optical phonons, the condition is not fulfilled as the density ratio is much more than 1.5 times as discussed above. If the phonons are acoustic phonons, only the second order perturbation approach will lead to the gap independence. Therefore, we consider that the 1st order perturbation approach[15] is less likely a reason for the observed energy gap independence.

### 4.6 Temperature dependent vibrational energy transfers in crystals

#### 4.6.1 Energy transfers in KS$^{13}$C$^{15}$N/KSCN = 1/1 mixed crystal.

As discussed above, the experimentally observed nonresonant energy transfer from CN to $^{13}$C$^{15}$N in the KS$^{13}$C$^{15}$N/KSCN = 1/1 mixed crystal must be mainly determined by the phonon compensation mechanism. This argument can be tested with temperature dependent experiments. According to eqn (24), if the conclusion is valid, the energy transfer rate constant $k_{CN\rightarrow{}^{13}C^{15}N}$ from CN to $^{13}$C$^{15}$N must be proportional to $[\exp(|\Delta E|/k_BT) - 1]^{-1} + 1$ where $\Delta E$ = 75 cm$^{-1}$, provided that

Published on 20 May 2014. Downloaded by Peking University on 9/2/2022 10:14:10 AM.

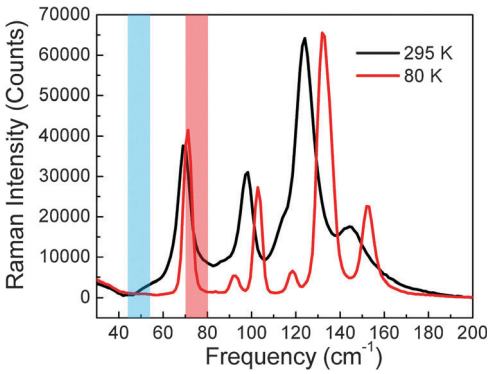


Fig. 9 Raman spectra of KSCN crystal at 295 K and 80 K. The two columns indicate the two energy gaps.

there are no coupling or phonon mode changes. Temperature dependent neutron diffraction studies show that in KSCN crystals no phase transitions occur between 80 K to 295 K, but the unit cell volume shrinks at a lower temperature with a volume ratio 1.04/1.01/1 (295 K/150 K/80 K).[57] According to eqn (5), (24) and (26), the volume change leads to a small energy transfer rate change with a ratio of 1.08/1.02/1 (295 K/150 K/80 K). Raman scattering measurements in Fig. 9 shows that the phonon modes around 70–75 $cm^{-1}$ exist at both room temperature and at 80 K, with the line width becoming a little narrower and the center frequency slightly blueshifting. Such small frequency changes are expected to not affect the energy transfer rate from CN to $^{13}C^{15}N$ very much as the FWHM of the nitrile stretch peak is 10 $cm^{-1}$. Therefore, we expect that the temperature dependence of the energy transfer from CN to $^{13}C^{15}N$ should follow $[\exp(|\Delta E|/k_BT) - 1]^{-1} + 1$ reasonably well from 80 K to 295 K. The situation for the energy transfer from CN to $^{13}CN$ is very different. At about 50 $cm^{-1}$, the absorption peak which is probably the shoulder of the major peak ~70 $cm^{-1}$ almost completely disappears at 80 K. If the phonon densities involved in the energy transfer process are correlated with spectral intensities observed in Fig. 9, we expect that the energy transfer from CN to $^{13}CN$ at 80 K compared to that at 295 K must be much slower than that predicted by $[\exp(|\Delta E|/k_BT) - 1]^{-1} + 1$.

Vibrational energy exchange measurements (Fig. 10) show that the energy transfer time from CN to $^{13}C^{15}N$ is $\frac{1}{k_{CN\rightarrow{}^{13}C^{15}N}} =$ 163 ps at 150 K and $\frac{1}{k_{CN\rightarrow{}^{13}C^{15}N}} = 237$ ps at 80 K. Combining $\frac{1}{k_{CN\rightarrow{}^{13}C^{15}N}} = 99$ ps at 295 K, the experimentally measured energy transfer rate ratios at the three temperatures are 1/1.45/2.37 (80 K/150 K/295 K). The predicted rate ratio by $[\exp(|\Delta E|/k_BT) - 1]^{-1} + 1$ with the CN/$^{13}C^{15}N$ gap $\Delta E$ = 75 $cm^{-1}$ is 1/1.43/2.38 (80 K/150 K/295 K). Within experimental uncertainty (~5%), the experimental temperature dependence is identical to the predicted one. Combined with the discussion in Section 4.5, the results strongly support that the experimentally observed energy transfer from CN to $^{13}C^{15}N$ in the KS$^{13}C^{15}N$/KSCN = 1/1 mixed crystal is mainly determined by the phonon compensation mechanism. This temperature dependence also suggests that the phonon compensation process involves only one-phonon as processes with more phonons have different temperature dependences.[32,35] For example, if the process involves two phonons at 35 $cm^{-1}$ and 40 $cm^{-1}$, the temperature dependent energy transfer rate ratio would be 8.7/1 (295 K/80 K). This is very different from the prediction of one-phonon process 2.38/1 which is identical to the experimental value.

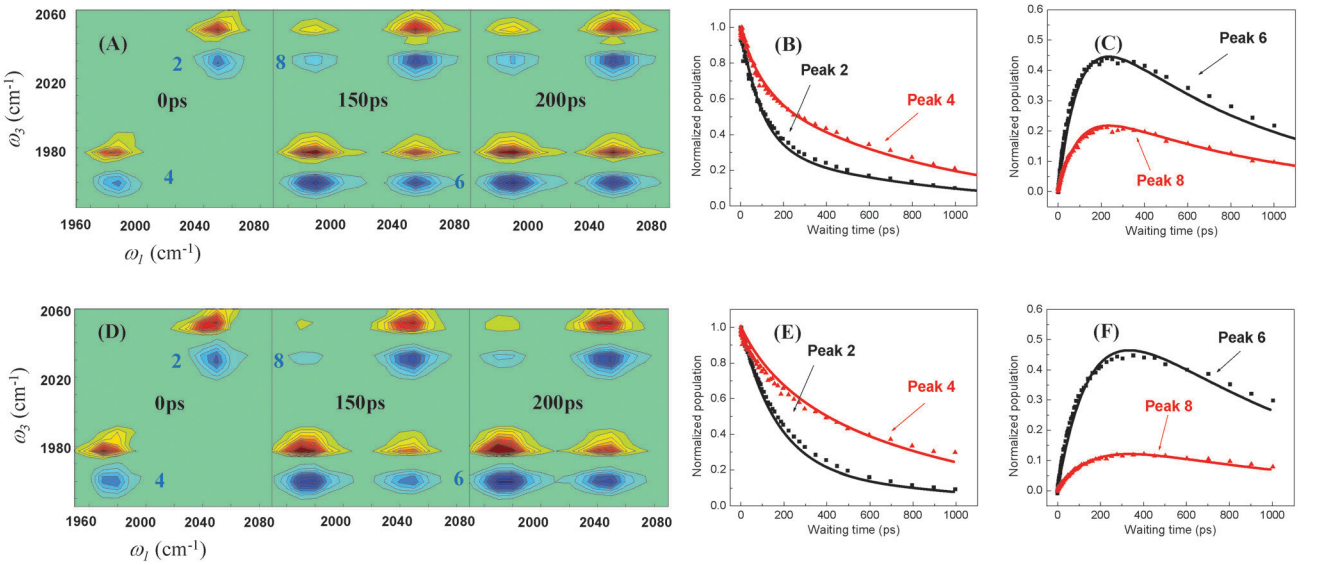


Fig. 10 (A) 2D IR spectra of a KSCN/KS$^{13}C^{15}N$ = 1/1 mixed crystal at 150 K at three waiting times; (B) and (C) the waiting time dependent intensities of peaks 2, 4, 6, 8 in (A). Dots are experimental results, and lines are kinetic model calculations. (D) 2D IR spectra of a KSCN/KS$^{13}C^{15}N$ = 1/1 mixed crystal at 80 K at three waiting times; (E) and (F) the waiting time dependent intensities of peaks 2, 4, 6, 8 in (D). Dots are experimental results, and lines are kinetic model calculations.

 This journal is © the Owner Societies 2014

Published on 20 May 2014. Downloaded by Peking University on 9/2/2022 10:14:10 AM.

**4.6.2 Energy transfers in KS$^{13}$CN/KSCN = 1/1 mixed crystal.** As discussed in Section 4.5, if the acoustic phonon with the Debye approximation is assumed, the energy transfer rate would be energy donor–acceptor gap independent. At room temperature, the observed energy transfers with gaps 48 cm$^{-1}$ and 75 cm$^{-1}$ are very similar. However, at lower temperatures *e.g.* 150 K and 80 K, the energy transfer times at these two gaps are very different. The results cannot be explained by the acoustic phonon assumption. As measured (in Fig. 11A–C), the energy transfer time from CN to $^{13}$CN at 150 K is $\frac{1}{k_{CN\rightarrow{}^{13}CN}} = 296$ ps, substantially longer than that (163 ps) from CN to $^{13}$C$^{15}$N at the same temperature. At 80 K, the difference is even larger. The energy transfer time from CN to $^{13}$CN is $\frac{1}{k_{CN\rightarrow{}^{13}CN}} = 636$ ps, about three times of that (237 ps) from CN to $^{13}$C$^{15}$N. Now the energy transfer is faster with a larger gap, opposite to those in the liquids discussed above. If we use the energy transfer time $\frac{1}{k_{CN\rightarrow{}^{13}CN}} = 96$ ps at 300 K as the starting point to estimate the time at 80 K using $[\exp(|\Delta E|/k_BT) - 1]^{-1} + 1$, the energy transfer time at 80 K would be $\frac{1}{k_{CN\rightarrow{}^{13}CN}} = 259$ ps. The predicted value is more than two times faster than that (636 ps) experimentally observed. The Raman spectra in Fig. 9 provide a very likely explanation for this result. At room temperature, the phonon to compensate the energy gap 48 cm$^{-1}$ between CN and $^{13}$CN is provided by the shoulder of the phonon (probably optical phonons) modes of ~70 cm$^{-1}$. At 80 K, because the central frequency of the phonon modes blueshifts and the peak becomes narrower, the shoulder of the phonon modes is very small at 48 cm$^{-1}$ so that the phonon density to compensate the energy gap is small and the energy transfer accordingly slows down. Here we want to point out that the discussion is based on the assumption that the phonon density involved in the energy transfer is correlated with the observed Raman intensity. The assumption does not necessarily reflect the truth as the assumed phonon density change (change for ~6 times from RT to 80 K) is much larger than that of the structural change (4% volume change from RT to 80 K).

There can be an alternative explanation for the slow energy transfers from CN to $^{13}$CN at low temperatures: the dephasing mechanism. If the energy transfer is determined by the dephasing mechanism, the energy transfer dephasing time $\tau$ needs to slow down for about 3 times from room temperature to 150 K and 6.4 times to 80 K. However, such huge dephasing time changes are not easy to imagine as no phase transformations or significant structural changes occur in the temperature range, especially compared to the 17% change of dephasing time in the aqueous solution from room temperature to 80 °C described above.

Neither explanation is completely satisfactory. The phonon density loss at 48 cm$^{-1}$ at low temperatures is probably a very important reason for the observed slow energy transfers at low temperatures, but the dephasing mechanism also plays a significant role as the estimated transfer rate at RT based on eqn (5) is about 30% to 80% of the measured rate. In principle, this issue can be further tested with temperature dependent resonant energy transfer measurements (Fig. S2 in ESI†). However, based on eqn (5), in order for $\frac{1}{k_{CN\rightarrow{}^{13}CN}} = 296$ ps (150 K) and 636 ps (80 K), the energy transfer dephasing widths need to be 2.8 cm$^{-1}$ and 1.4 cm$^{-1}$ respectively. These two values are already smaller than two times (4.6 cm$^{-1}$) the largest coupling

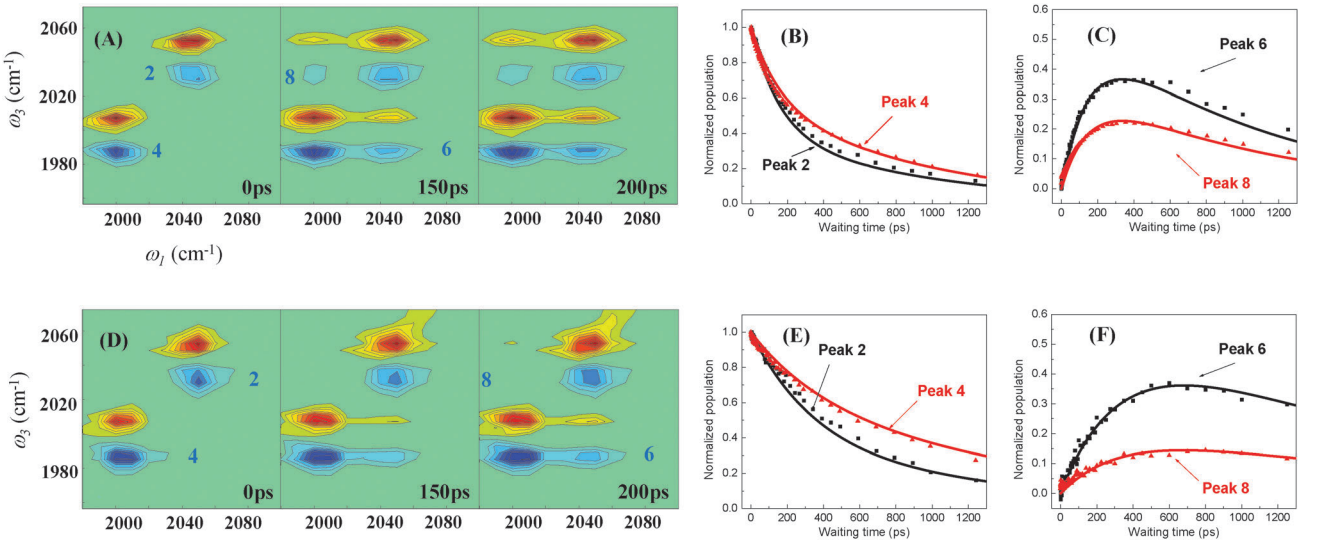


Fig. 11 (A) 2D IR spectra of a KSCN/KS$^{13}$CN = 1/1 mixed crystal at 150 K at three waiting times; (B) and (C) the waiting time dependent intensities of peaks 2, 4, 6, 8 in (A). Dots are experimental results, and lines are kinetic model calculations. (D) 2D IR spectra of a KSCN/KS$^{13}$CN = 1/1 mixed crystal at 80 K at three waiting times; (E) and (F) the waiting time dependent intensities of peaks 2, 4, 6, 8 in (D). Dots are experimental results, and lines are kinetic model calculations.

Published on 20 May 2014. Downloaded by Peking University on 9/2/2022 10:14:10 AM.

strength between two adjacent anions in the KSCN crystal. Under such a circumstance, using eqn (5) to predict resonant energy transfer can introduce nontrivial uncertainties as the energy transfer can go through the coherent process of which the energy transfer rate only slightly (or does not, under the perfect condition) depends on the dephasing time.[24] As we can see from Fig. S2 in ESI,† the resonant energy transfer only becomes slightly faster (~30%) from room temperature down to 80 K. There can be a third possible explanation for the observed huge temperature dependence. According to a previous nonlinear theory of dephasing on energy transfer rates,[36–38] a more dramatic increase in the energy transfer rate with increasing dephasing rate is expected when the latter is not very large, *e.g.* at 80 K, with a smaller increase at a larger dephasing rate, *e.g.* 295 K. Such an effect can be more dramatic in the 1/1 mixed crystal with a smaller gap (48 $cm^{-1}$) than in the mixed crystal with a larger gap (75 $cm^{-1}$).

**4.6.3 Nonresonant vibrational energy transfer in mixed crystals of KSCN/KS$^{13}$C$^{15}$N of different ratios.** There can be a concern that in the mixed crystals of KSCN and its isotope-labeled species KSCN or the other species can form individual domains so that the energy transfers may not follow the exact molar ratio of the two species. To address this issue, we measured the vibrational energy exchanges (Fig. 12) in two mixed crystals of KSCN/KS$^{13}$C$^{15}$N with 3/7 and 7/3 molar ratios at room temperature, in addition to the 1/1 sample discussed above. Analyses show that in the KSCN/KS$^{13}$C$^{15}$N = 3/7 sample, the CN to $^{13}$C$^{15}$N energy transfer time is $\frac{1}{k_{CN\rightarrow{}^{13}C^{15}N}} = 68 \pm 5$ ps and the reverse transfer time is $\frac{1}{k_{{}^{13}C^{15}N\rightarrow CN}} = 240 \pm 10$ ps. In the KSCN/KS$^{13}$C$^{15}$N = 7/3 sample, the CN to $^{13}$C$^{15}$N energy transfer time is $\frac{1}{k_{CN\rightarrow{}^{13}C^{15}N}} = 162 \pm 8$ ps and the reverse transfer time is $\frac{1}{k_{{}^{13}C^{15}N\rightarrow CN}} = 104 \pm 5$ ps. The transfer forward and backward rate constant ratios in both samples can be described by the equation

$$\frac{k_{DA}}{k_{AD}} = e^{\frac{E_D - E_A}{RT}} \times \frac{n_A}{n_D}, \quad (27)$$

where $k_{DA}$ and $k_{AD}$ are the transfer rates from D to A and from A to D respectively, $E_D$ and $E_A$ are the energy values of D and A respectively, and $n_D$ and $n_A$ are the numbers of D and A. Eqn (27) is based on the fact that in a typical nonlinear IR experiment, only less than 5% of the molecules are vibrationally excited by the lasers. Therefore, for a D/A ratio larger than the ratio of molecules that are laser-excited, the relative number of the energy acceptors for one donor in a series of experiments is only determined by the concentration of the acceptors. For instances, in the three KSCN/KS$^{13}$C$^{15}$N mixed samples, the concentrations of S$^{13}$C$^{15}$N$^-$ are 30% (KSCN/KS$^{13}$C$^{15}$N = 7/3), 50% (KSCN/KS$^{13}$C$^{15}$N = 1/1) and 70% (KSCN/KS$^{13}$C$^{15}$N = 3/7). For the energy transfer from CN to $^{13}$C$^{15}$N, the ratio of the number of energy acceptors in the three samples is 3/5/7. Therefore, the energy transfer time ratio must also be 7/5/3. Experimentally, the ratio is 162/99/68 = 7.1/4.4/3. The experimental ratio is very close to the predicted ratio, indicating that in the mixed crystalline samples the effect of micron domains of single species (if any) on the energy transfer rates is statistically averaged. This result can be explained in another way. The chemical properties of KSCN and its isotope-labeled counterparts are essentially identical, and therefore the probability at any physical location in the sample is the same for each species. This naturally leads to the linear relationship between the number of the acceptors and the concentration of the species other than the donor.

In summary, using the crystalline samples, we were able to quantitatively test the dephasing mechanism with resonant vibrational energy transfers. We were also able to demonstrate two different energy gap dependences of the nonresonant vibrational energy transfers. The observed energy gap dependence and the

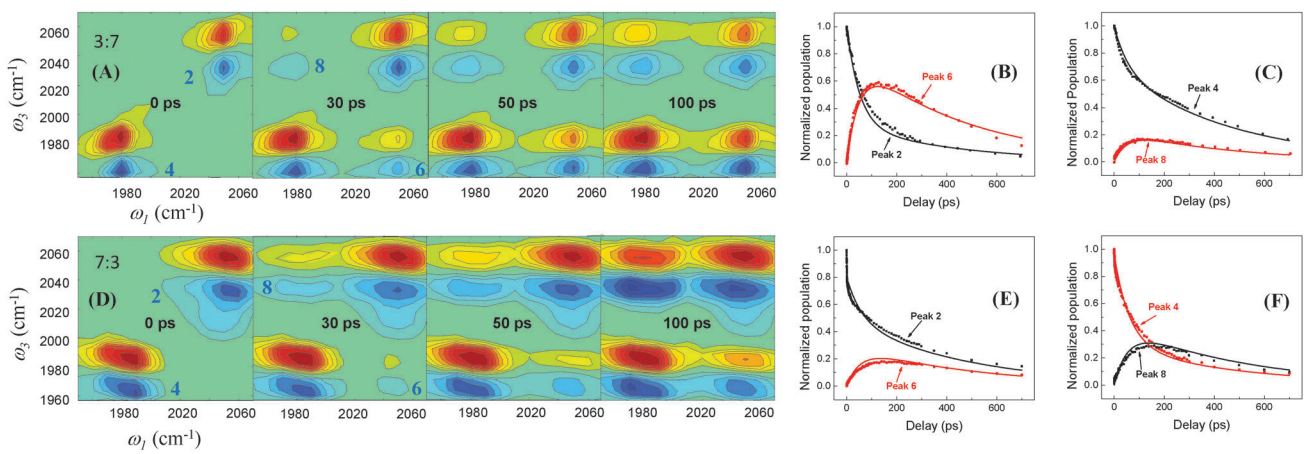


Fig. 12 (A) 2D IR spectra of a KSCN/KS$^{13}$C$^{15}$N = 3/7 mixed crystal at 295 K at four waiting times; (B) and (C) the waiting time dependent intensities of peaks 2, 4, 6, 8 in (A). Dots are experimental results, and lines are kinetic model calculations. (D) 2D IR spectra of a KSCN/KS$^{13}$C$^{15}$N = 7/3 mixed crystal at 295 K at four waiting times; (E) and (F) the waiting time dependent intensities of peaks 2, 4, 6, 8 in (D). Dots are experimental results, and lines are kinetic model calculations. In each 2D IR spectrum, the diagonal peaks are normalized to 1, and the corresponding cross peaks along the *y*-axis are normalized accordingly.

 This journal is © the Owner Societies 2014

Published on 20 May 2014. Downloaded by Peking University on 9/2/2022 10:14:10 AM.

temperature dependence of vibrational energy transfers of the KSCN/$KS^{13}C^{15}N$ = 1/1 mixed crystal can be described by eqn (24) of the phonon compensation mechanism reasonably well. The temperature dependence of energy transfers of the KSCN/$KS^{13}CN$ = 1/1 mixed crystal is probably the sum result of both mechanisms. The dependences are hard to explain by the phonon compensation mechanism of the first order perturbation approach unless some specific conditions which seem to be less reasonable (compared to those for eqn (24)) are assumed.

## 5. Concluding remarks

In this work, we systematically studied intermolecular vibrational energy transfers in liquids and crystalline solids. We found that in both liquid and solid samples, the resonant energy transfers are faster at a lower temperature but the nonresonant energy transfers are slower at a lower temperature. In liquids, at the same temperature, the nonresonant energy is faster if the donor–acceptor energy gap is smaller. In solids, dependent on the temperature, the nonresonant energy transfers can be faster with a larger donor–acceptor energy gap or energy gap independent. To explain the experimental observations, we proposed two energy transfer mechanisms: the dephasing mechanism which is essentially dependent on the probability of the donor being resonant with the acceptor caused by the dephasing events; and the phonon compensation mechanism of the second order perturbation that is dependent on the environment to provide phonons to compensate the donor–acceptor energy gap. In the first mechanism, the probability of donor–acceptor on resonance physically exists. In the second mechanism, the phonon compensation is through the ''virtual intermediate states'' which do not physically exist. The experimental results in the liquid samples and the resonant energy transfer data in the solid samples are well explained by the dephasing mechanism. The quantitative nature of this mechanism also allows the donor–acceptor distance to be derived from the vibrational energy transfer rate measurements (combined with the transition dipole–transition dipole interaction). The nonresonant vibrational energy transfer experiments in the solid samples can be reasonably described by the phonon compensation mechanism. We expect that both energy transfer mechanisms simultaneously play roles in nonresonant vibrational energy transfers in condensed phases. Which mechanism is dominant is dependent on the detailed situation. Based on our results, our tentative opinion is that since the essential differences in liquid and crystalline solid samples are that in solids there can be many more well defined phonon modes but in liquids the dephasing is typically faster, in liquids the dephasing mechanism is probably dominant if no specific phonon modes exist in the frequency range of the donor–acceptor gap for relatively small gaps (*e.g.* $\Delta\omega < RT$). In solids, the phonon compensation mechanism can be important in samples where many phonon modes at the donor–acceptor energy gaps exist. One unsatisfactory point of the phonon compensation mechanism is that the phonon/system coupling and the phonon densities involved in the energy transfer process are very difficult to be experimentally obtained. How to solve this issue is the subject of future studies.

## Conflicts of interest

The authors declare no competing financial interest.

## Acknowledgements

This material is based upon work supported by the Welch foundation under Award No. C-1752 and AFOSR Award No. FA9550-11-1-0070. J. R. Zheng also thanks the David and Lucile Packard Foundation for a Packard fellowship. Insightful discussions with Profs Robert, F. Curl, Peter Wolynes, Anatoly B. Kolomeisky, David Jonas, Greg Angel, James Hynes, Wei Yang, Yi-qin Gao, and Zhigang Sun are appreciated.

## References

1 D. W. Oxtoby, *Annu. Rev. Phys. Chem.*, 1981, **32**, 77–101.
2 A. Laubereau, L. Kirschner and W. Kaiser, *Opt. Commun.*, 1973, **9**, 182–185.
3 A. Laubereau and W. Kaiser, *Rev. Mod. Phys.*, 1978, **50**, 607.
4 D. W. Oxtoby, *Adv. Chem. Phys.*, 1981, **47**, 487–519.
5 E. L. Sibert, W. P. Reinhardt and J. T. Hynes, *J. Chem. Phys.*, 1984, **81**, 1115–1134.
6 X. Y. Hong, S. Chen and D. D. Dlott, *J. Phys. Chem.*, 1995, **99**, 9102–9109.
7 A. Tokmakoff, B. Sauter and M. D. Fayer, *J. Chem. Phys.*, 1994, **100**, 9035.
8 S. A. Egorov and J. L. Skinner, *J. Chem. Phys.*, 1996, **105**, 7047–7058.
9 H. J. Bakker, *J. Chem. Phys.*, 1993, **98**, 8496.
10 R. M. Stratt, *Acc. Chem. Res.*, 1995, **28**, 201–207.
11 J. C. Owrutsky, D. Raftery and R. M. Hochstrasser, *Annu. Rev. Phys. Chem.*, 1994, **45**, 519.
12 E. L. Sibert and R. Rey, *J. Chem. Phys.*, 2002, **116**, 237–257.
13 M. Yang, F. Li and J. L. Skinner, *J. Chem. Phys.*, 2011, **135**, 10.
14 J. L. Skinner, *Theor. Chem. Acc.*, 2011, **128**, 147–155.
15 V. M. Kenkre, A. Tokmakoff and M. D. Fayer, *J. Chem. Phys.*, 1994, **101**, 10618–10629.
16 H. T. Bian, X. W. Wen, J. B. Li and J. R. Zheng, *J. Chem. Phys.*, 2010, **133**, 034505.
17 H. Bian, J. Li, X. Wen and J. R. Zheng, *J. Chem. Phys.*, 2010, **132**, 184505.
18 H. T. Bian, H. L. Chen, J. B. Li, X. W. Wen and J. R. Zheng, *J. Phys. Chem. A*, 2011, **115**, 11657–11664.
19 H. T. Bian, X. W. Wen, J. B. Li, H. L. Chen, S. Z. Han, X. Q. Sun, J. A. Song, W. Zhuang and J. R. Zheng, *Proc. Natl. Acad. Sci. U. S. A.*, 2011, **108**, 4737–4742.
20 H. T. Bian, J. B. Li, Q. Zhang, H. L. Chen, W. Zhuang, Y. Q. Gao and J. R. Zheng, *J. Phys. Chem. B*, 2012, **116**, 14426–14432.
21 J. B. Li, H. T. Bian, X. W. Wen, H. L. Chen, K. J. Yuan and J. R. Zheng, *J. Phys. Chem. B*, 2012, **116**, 12284–12294.

Published on 20 May 2014. Downloaded by Peking University on 9/2/2022 10:14:10 AM.

22 J. B. Li, H. T. Bian, H. L. Chen, B. Hoang and J. R. Zheng, *J. Phys. Chem. B*, 2013, **117**, 4274–4283.
23 D. Laage, H. Demirdjian and J. T. Hynes, *Chem. Phys. Lett.*, 2005, **405**, 453–458.
24 J. A. Leegwater, *J. Phys. Chem.*, 1996, **100**, 14403–14409.
25 H. L. Chen, H. T. Bian, J. B. Li, X. M. Guo, X. W. Wen and J. R. Zheng, *J. Phys. Chem. B*, 2013, **117**, 15614–15624.
26 T. Förster, *Ann. Phys.*, 1948, **2**, 55.
27 D. L. Dexter, *J. Chem. Phys.*, 1953, **21**, 836–850.
28 T. Miyakawa and D. L. Dexter, *Phys. Rev. B: Solid State*, 1970, **1**, 2961–2969.
29 A. Nitzan and R. J. Silbey, *J. Chem. Phys.*, 1974, **60**, 4070–4075.
30 S. Rackovsky and R. Silbey, *Mol. Phys.*, 1973, **25**, 61–72.
31 A. Nitzan, S. Mukamel and J. Jortner, *J. Chem. Phys.*, 1975, **63**, 200–207.
32 T. Holstein, S. K. Lyo and R. Orbach, *Laser spectroscopy of solids*, Springer, New York, 1986, pp. 39–82.
33 A. A. Stuchebrukhov and R. A. Marcus, *J. Chem. Phys.*, 1993, **98**, 6044–6061.
34 S. H. Lin, *J. Chem. Phys.*, 1976, **65**, 1053–1062.
35 S. A. Egorov and J. L. Skinner, *J. Chem. Phys.*, 1995, **103**, 1533–1543.
36 D. E. Logan and P. G. Wolynes, *J. Chem. Phys.*, 1990, **93**, 4994–5012.
37 D. E. Logan and P. G. Wolynes, *J. Chem. Phys.*, 1987, **87**, 7199–7207.
38 D. M. Leitner, *New J. Phys.*, 2010, **12**, 085004.
39 R. F. Curl, J. V. V. Kasper and K. S. Pitzer, *J. Chem. Phys.*, 1967, **46**, 3220–3228.
40 H. L. Chen, X. W. Wen, J. B. Li and J. R. Zheng, *J. Phys. Chem. A*, 2014, **118**, 2463–2469.
41 J. Zheng, K. Kwak and M. D. Fayer, *Acc. Chem. Res.*, 2007, **40**, 75–83.
42 J. Zheng, K. Kwak, J. B. Asbury, X. Chen, I. Piletic and M. D. Fayer, *Science*, 2005, **309**, 1338–1343.
43 J. Zheng and M. D. Fayer, *J. Phys. Chem. B*, 2008, **112**, 10221.
44 O. Golonzka, M. Khalil, N. Demirdoven and A. Tokmakoff, *Phys. Rev. Lett.*, 2001, **86**, 2154–2157.
45 M. Khalil, N. Demirdoven and A. Tokmakoff, *J. Phys. Chem. A*, 2003, **107**, 5258–5279.
46 Y. S. Kim and R. M. Hochstrasser, *Proc. Natl. Acad. Sci. U. S. A.*, 2005, **102**, 11185–11190.
47 S. A. Egorov and B. J. Berne, *J. Chem. Phys.*, 1997, **107**, 6050–6061.
48 R. Zwanzig, *J. Chem. Phys.*, 1961, **34**, 1931–1935.
49 H. L. Chen, H. T. Bian, J. B. Li, X. W. Wen and J. R. Zheng, *Int. Rev. Phys. Chem.*, 2012, **31**, 469–565.
50 G. D. Scholes, *Annu. Rev. Phys. Chem.*, 2003, **54**, 57–87.
51 J. C. Chang, *J. Chem. Phys.*, 1977, **67**, 3901–3909.
52 S. Woutersen and H. J. Bakker, *Nature*, 1999, **402**, 507–509.
53 I. Natkaniec, L. S. Smirnov and A. I. Solovev, *Physica B*, 1995, **213**, 667–668.
54 H. T. Bian, H. L. Chen, Q. Zhang, J. B. Li, X. W. Wen, W. Zhuang and J. R. Zheng, *J. Phys. Chem. B*, 2013, **117**, 7972–7984.
55 C. Akers, S. W. Peterson and R. D. Willett, *Acta Crystallogr., Sect. B: Struct. Crystallogr. Cryst. Chem.*, 1968, **24**, 1125–1126.
56 D. J. Cookson, M. M. Elcombe and T. R. Finlayson, *J. Phys.: Condens. Matter*, 1992, **4**, 7851–7864.
57 L. S. Smirnov, I. Natkaniec, Y. A. Shadrin and A. I. Solov'ev, *Acta Phys. Hung.*, 1994, **75**, 275–278.

 This journal is © the Owner Societies 2014